



24 concentrations are moderately overpredicted with an NMB of 23.3% at rural sites, but slightly  
25 underpredicted with an NMB of -10.8% at urban/suburban sites. In general, the model performs  
26 relatively well for chemical and meteorological variables, and not as well for aerosol-cloud-  
27 radiation variables. Cloud-aerosol variables including aerosol optical depth, cloud water path,  
28 cloud optical thickness, and cloud droplet number concentration are generally underpredicted on  
29 average across the continental U.S. Overpredictions of several cloud variables over eastern U.S.  
30 result in underpredictions of radiation variables (such as GSW with an MB of  $-5.7 \text{ W m}^{-2}$ ) and  
31 overpredictions of shortwave and longwave cloud forcing (MBs of  $\sim 7$  to  $8 \text{ W m}^{-2}$ ) which are  
32 important climate variables. While the current performance is deemed to be acceptable,  
33 improvements to the bias-correction method for CESM downscaling and the model  
34 parameterizations of cloud dynamics and thermodynamics, as well as aerosol-cloud interactions  
35 can potentially improve model performance for long-term climate simulations.

36 **KEYWORDS:** Online-Coupled WRF/Chem; Climate, Air Quality, the Representative  
37 Concentration Pathway Scenarios, Climatological Evaluation; Chemistry-Climate Interactions

## 38 **1. Introduction**

39 Regional atmospheric models have been developed and applied for high resolution climate,  
40 meteorology, and air quality modeling in the past few decades. Comparing to global models with  
41 a coarser domain resolution (Leung et al., 2003) those regional models have advantages over  
42 global models because they can more accurately represent mesoscale variability (Feser et al.,  
43 2011), and also better predict the local variability of concentrations of specific species such as  
44 black carbon and sulfate (Petikainen et al., 2012). General circulation models (GCMs) and global  
45 chemical transport models (GCTMs) are usually downscaled to regional meteorological models  
46 such as the Weather Research and Forecasting model (WRF) (Caldwell et al., 2009; Gao et al.,

47 2012), regional climate models such as REMO-HAM (Petikainen et al., 2012), the regional  
48 modeling system known as Providing Regional Climates for Impacts Studies (PRECIS) (Jones et  
49 al., 2004; Fan et al., 2014), and a number of European models described in Jacob et al. (2007), as  
50 well as regional CTMs such as the Community Multiscale Air Quality Model (CMAQ) (Penrod et  
51 al., 2014; Xing et al., 2015). These regional models are used for climate/meteorology or air quality  
52 simulations. Some are applied for more than ten years (Caldwell et al., 2009; Warrach-Sagi et al.,  
53 2013; Xing et al., 2015). However these regional models either lack the detailed treatment of  
54 chemistry (e.g., in WRF), or use prescribed chemical concentrations (e.g., REMO-HAM uses  
55 monthly mean oxidant fields for several chemical species), or do not have online-coupled  
56 meteorology and chemistry (e.g., in CMAQ). In addition, the past regional model simulations and  
57 analyses have mainly focused on meteorological parameters such as surface temperature and  
58 precipitation, cloud variables such as net radiative cloud forcing, and chemical constituents such  
59 as ozone. Regional climate model simulations tend to focus on significant climatic events such as  
60 extreme temperatures (very cold or very hot) (Dasari et al., 2014), heat waves, heavy precipitation,  
61 drought, and storms (Beniston et al., 2007), rather than the important air quality and climate  
62 interactions. In addition, the impacts of complex chemistry-aerosol-cloud-radiation-climate  
63 feedbacks on future climate change remain uncertain, and these feedbacks are most accurately  
64 represented using online-coupled meteorology and chemistry models (Zhang, 2010; IPCC, 2013).  
65 An online-coupled meteorology and chemistry model, however, is more computationally  
66 expensive compared to an offline-coupled model (Grell et al., 2004), and thus requires significant  
67 computing resources for their long-term (a decade or longer) applications. With rapid increases in  
68 the availability of high performance computing resources on the petaflop scale, however, long  
69 term simulations using online-coupled models have become possible in recent years. For example,

70 recently, the WRF model has been coupled online to the CMAQ model with the inclusion of  
71 aerosol indirect effects to study chemistry and climate interactions (Yu et al., 2014).

72         The online-coupled WRF model with Chemistry (WRF/Chem) has been updated with a  
73 suite of physical parameterizations from the Community Atmosphere Model version 5 (CAM5)  
74 (Neale et al., 2010) so that the physics in the global CAM5 model is consistent with the regional  
75 model for downscaling purposes (Ma et al., 2014). There are also limited applications of dynamical  
76 downscaling (Gao et al., 2013) under the new Intergovernmental Panel on Climate Change (IPCC)  
77 Fifth Assessment Report’s Representative Concentration Pathway (RCP) scenarios (van Vuuren  
78 et al., 2011). Gao et al. (2013) applied dynamic downscaling to link the global-climate-chemistry  
79 model CAM-Chem with WRF and CMAQ using RCP 8.5 and RCP 4.5 emissions to study the  
80 impacts of climate change and emissions on ozone (O<sub>3</sub>). Molders et al. (2014) downscaled the  
81 Community Earth System Model (CESM) (Hurrell et al., 2013) to drive the online-coupled  
82 WRF/Chem model over Southeast Alaska using RCP 4.5 emissions; however, their study did not  
83 address the feedback processes between chemistry and meteorology. This study evaluates the  
84 online-coupled regional WRF/Chem model, which takes into account gas and aerosol-phase  
85 chemistry, as well as aerosol direct and indirect effects. WRF/Chem is used to simulate the  
86 “current” climate scenario for 10 years, from 2001 to 2010 using the RCP 8.5 emissions and  
87 boundary conditions from an updated version of CESM with advanced chemistry and aerosol  
88 treatments over continental U.S. (CONUS) (He et al., 2015; Glotfelty et al., 2015) with a focus on  
89 air-quality and climate interactions. Both CESM and WRF/Chem include similar gas-phase  
90 chemistry and aerosol treatments. To our best knowledge, this study is the first to report the  
91 WRF/Chem simulation, evaluation, and analyses over a period of 10 years (i.e., 2001-2010) to  
92 assess if the model is able to accurately simulate decadal long air quality and climatology by taking

93 into account feedback processes between chemistry and meteorology. This study also assesses  
94 whether the RCP8.5 emissions for the 10-year period are robust enough to produce satisfactory  
95 performance against observations with WRF/Chem.

## 96 **2. Model Set-up and Evaluation Protocol**

### 97 **2.1 Model Configurations and Simulation Design**

98 The model used is the modified WRF/Chem v3.6.1 with updates similar to those  
99 implemented into WRF/Chem v3.4.1 as documented in Wang et al. (2014). The main updates  
100 include the implementation of an extended version of Carbon Bond 2005 (CB05) (Yarwood et al.,  
101 2005) gas-phase mechanism with the chlorine chemistry (Sarwar et al., 2007) and its coupling with  
102 the Modal for Aerosol Dynamics in Europe/Volatility Basis Set (MADE/VBS) (Ahmadov et al.,  
103 2012). MADE/VBS incorporates a modal aerosol size distribution, and includes an advanced  
104 secondary organic aerosol (SOA) treatment based on gas-particle partitioning and gas-phase  
105 oxidation in volatility bins. The CB05-MADE/VBS option has also been coupled to existing model  
106 treatments of various feedback processes such as the aerosol semi-direct effect on photolysis rates  
107 of major gases, and the aerosol indirect effect on cloud droplet number concentration (CDNC) and  
108 resulting impacts on shortwave radiation. The main physics and chemistry options used in this  
109 study as well as their corresponding references can be found in Table 1. The simulations are  
110 performed at a horizontal resolution of 36-km with  $148 \times 112$  horizontal grid cells over the  
111 CONUS domain and parts of Canada and Mexico, and a vertical resolution of 34 layers from the  
112 surface to 100-hPa. Considering the decadal applications of WRF/Chem in this work which is  
113 much longer than many past WRF/Chem applications, the simulations are reinitialized monthly  
114 (rather than 1-4 days used in most past WRF/Chem applications to short-term episodes that are on  
115 an order of months up to 1-year, e.g., Zhang et al., 2012a, b; Yahya et al., 2014, 2015b) to constrain

116 meteorological fields toward National Centers for Environmental Prediction (NCEP) reanalysis  
117 data while allowing chemistry-meteorology feedbacks within the system. As discussed in Sections  
118 3.1 and 3.3, the reinitialization frequency of 1-month may be too large to constrain some of the  
119 meteorological fields such as moistures, which in turn affect other parameters, and a more frequent  
120 reinitialization may be needed to improve the model performance. The impact of the frequency of  
121 the reinitialization on simulated meteorological and cloud parameters will be further discussed in  
122 Sections 3.1 and 3.2. A list of acronyms used in this paper can be found in Table S1.

## 123 **2.2 Processing of Emissions and Initial Conditions (ICs)/Boundary Conditions (BCs)**

124 Global RCP emissions are available as monthly-average emissions for 2000, 2005, and for  
125 every 10 years between 2010 and 2100, at a grid resolution of  $0.5^{\circ} \times 0.5^{\circ}$  (Moss et al., 2010; van  
126 Vuuren et al., 2011). The RCP emissions in 2000, 2005, and 2010 are used to cover the 10-year  
127 emissions needed for WRF/Chem simulations, i.e., the periods of 2001 – 2003, 2004 – 2006, and  
128 2007 – 2010, respectively. Processing global RCP emissions in 2000, 2005, and 2010 into regional,  
129 hourly emissions needed for the 10-year WRF/Chem simulations requires essentially three main  
130 tasks. These include 1) mapping the RCP species to CB05 speciation used in WRF/Chem; 2) re-  
131 gridding the RCP emissions from  $0.5 \times 0.5^{\circ}$  grid resolution to the  $36 \times 36$  km grid resolution used  
132 for regional simulation over North America; and 3) applying species and location dependent  
133 temporal allocations (i.e., emissions variation over time) to the re-gridded RCP emissions. Table  
134 S2 shows the species mapping between RCP species and CB05 species. To map the RCP species  
135 to CB05 speciation, some assumptions are made due the relatively detailed speciation required by  
136 CB05. Some of the CB05 species are directly available in RCP; however, others are lumped into  
137 RCP groups, for example, the “other alkanals” and “hexanes and higher alkanes” in the RCP  
138 groups can be considered to approximately represent the acetaldehyde and higher aldehydes

139 emissions required by CB05, respectively (Table S2). For the CB05 species such as ethanol,  
140 methanol, internal and terminal olefin carbon bonds in the gas-phase, and elemental and organic  
141 carbon in the accumulation mode of the aerosol particles, other RCP groups are used to  
142 approximate these emissions (Table S2). For the remaining CB05 species that are not available in  
143 RCP, the 2000 emissions are based on the 2002 National Emission Inventory (NEI) (version 3,  
144 <http://www.epa.gov/ttn/chief/emch/>), while the 2005 and 2010 emissions are based on the 2008  
145 NEI (version 2), with year-specific updates for on/off road transport, wildfires and prescribed fires,  
146 and Continuous Emission Monitoring-equipped point sources (Pouliot et al., 2014). To re-grid the  
147 RCP emissions, the RCP rectilinear grid is first interpolated to a WRF/Chem curvilinear grid using  
148 a simple inverse distance weighting (NCAR Command Language Function – rgrid2rcm), and a  
149 subset of the RCP grid that covers the WRF/Chem CONUS domain is then extracted. To derive a  
150 temporal allocation for monthly-averaged RCP emissions, hourly emissions profiles are taken  
151 from in-house WRF/Chem simulations over CONUS during 2001 (Yahya et al., 2015a), and 2006  
152 and 2010 (Yahya et al., 2014, 2015b). For those existing in-house simulations, the emissions were  
153 generated with the Sparse Matrix Operator Kernel Emissions (SMOKE) model version 2.3 for  
154 2002 NEI and SMOKE version 3.4 for 2008 NEI with year-specific sector emissions for 2006 and  
155 2010, which prepare the spatially, temporally, and chemically speciated “model-ready” emissions.  
156 Since NEI is updated and released every three years, the temporal profiles of emissions used in  
157 SMOKE for 2002, 2006 and 2010 are assumed to be valid for 3-4 years around the NEI years, i.e.,  
158 2001-2003, 2004-2006, and 2007-2010, respectively. The temporal allocations applied to the RCP  
159 emissions are therefore based on the SMOKE model’s profiles for each species and source  
160 location, and include non-steady-state emissions rates (i.e., seasonal, weekday or weekend, and

161 diurnal variability) that are valid for the entire simulation periods of 2001-2010. Specifically, the  
162 hourly re-gridded RCP emission rates for each species  $E$ , or  $E_{hr}^{RCP}$  are calculated by

$$163 \quad E_{hr}^{RCP}(t, z, \text{lat}, \text{lon}) = E_{mon}^{RCP}(z, \text{lat}, \text{lon}) * \left[ \frac{E_{hr}^{WRF}(t, z, \text{lat}, \text{lon})}{E_{mon}^{WRF}(z, \text{lat}, \text{lon})} \right] \quad (1)$$

164 where  $E_{mon}^{RCP}$ ,  $E_{mon}^{WRF}$ , and  $E_{hr}^{WRF}$  represent the original monthly-averaged RCP emissions rates, the  
165 monthly-averaged WRF/Chem emissions rates, and the hourly WRF/Chem emission rates,  
166 respectively, which are valid at each model time  $t$ , layer  $z$ , and  $lat$  and  $lon$  grid points. The RCP  
167 elevated source emissions for sulfur dioxide ( $\text{SO}_2$ ), sulfate ( $\text{SO}_4^{2-}$ ), elemental carbon (EC) and  
168 organic carbon (OC) were also incorporated into the model-ready emissions for WRF/Chem using  
169 steps 1) – 3) and Eq. (1) above. Lastly, RCP aircraft source emissions for EC, nitric oxide (NO),  
170 and nitrogen dioxide ( $\text{NO}_2$ ) are directly injected into the closest model layers. No temporal  
171 allocations are applied to the RCP aircraft source emissions.

172 Biogenic emissions are calculated online using the Model of Emissions of Gases and  
173 Aerosols from Nature version 2 (MEGAN2) (Guenther et al., 2006). Emissions from dust are based  
174 on the online Atmospheric and Environmental Research Inc. and Air Force Weather Agency  
175 (AER/AFWA) scheme (Jones and Creighton, 2011). Emissions from sea salt are generated based  
176 on the scheme of Gong et al. (1997).

177 The chemical and meteorological ICs/BCs come from the modified CESM/CAM5 version  
178 1.2.2 with updates by He et al. (2014) and Glotfelty et al. (2015) developed at the North Carolina  
179 State University (CESM\_NCSU). WRF/Chem and CESM both use the CB05 gas-phase  
180 mechanism (Yarwood et al., 2005), however, WRF/Chem includes additional chlorine chemistry  
181 from Sarwar et al. (2007), whereas CESM\_NCSU uses a modified version of CB05, the CB05  
182 Global Extension (CB05GE) by Karamchandani et al. (2012). In addition to original reactions in

183 CB05 and chlorine chemistry of Sarwar et al. (2007), CB05GE includes chemistry on the lower  
184 stratosphere, reactions involving mercury species, and additional heterogeneous reactions on  
185 aerosol particles, cloud droplets and on polar stratospheric clouds (PSCs). Both WRF/Chem and  
186 CESM\_NCSU use a modal aerosol size representation, rather than a sectional size representation.  
187 While WRF/Chem includes MADE/VBS with 3 prognostic modes (Ahmadov et al.,  
188 2012),CESM\_NCSU includes the Modal Aerosol Model with 7 prognostic modes (Liu et al., 2012)  
189 is used in CESM\_NCSU. In addition to similar gas-phase chemistry and aerosol treatments,  
190 CESM\_NCSU and WRF/Chem use the same shortwave and longwave radiation schemes (i.e., the  
191 Rapid and accurate Radiative Transfer Model for GCM (RRTMG)), though they use different  
192 cloud microphysics parameterizations, PBL, and convection schemes. As GCMs generally contain  
193 systematic biases which can influence the downscaled simulation, the meteorological ICs/BCs  
194 predicted by CESM\_NCSU are bias corrected before they are used by WRF/Chem using the  
195 simple bias correction technique based on Xu and Yang (2012). Temperature, water vapor,  
196 geopotential height, wind, and soil moisture variables available every 6 hours from the NCEP Final  
197 Reanalyses (NCEP FNL) dataset are used to correct the ICs and BCs derived based on results from  
198 CESM\_NCSU for WRF/Chem simulations. In this bias-correction approach, monthly  
199 climatological averages for ICs and BCs are first derived from both NCEP and CESM\_NCSU  
200 cases. The differences between the ICs and BCs from the NCEP and CESM\_NCSU climatological  
201 averages are then added onto the CESM\_NCSU ICs and BCs to generate bias-corrected  
202 CESM\_NCSU ICs/BCs. This bias correction technique can also be applied to future year  
203 simulations where NCEP FNL data is not available.

### 204 **2.3 Model Evaluation Protocol**

205           The focus of the model evaluation is mainly to assess whether the model is able to  
206 adequately reproduce the spatial and temporal distributions of key meteorological and chemical  
207 variables as compared to observations on a climatological time scale. A scientific question to be  
208 addressed in this work is, is WRF/Chem sufficiently good for regional climate and air quality  
209 simulations on a decadal scale? A climatological month refers to the average of the month for all  
210 the 10 years. For example, January refers to the average for all the months of January from 2001  
211 to 2010. Statistical evaluations such as mean bias (MB), Pearson's correlation coefficient (R),  
212 normalized mean bias (NMB), normalized mean error (NME) (The definition of those measures  
213 can be found in Yu et al. (2006) and Zhang et al. (2006)) and Index of Agreement (IOA) ranging  
214 from 0 to 1 (Willmott et al., 1981) for major chemical and meteorological variables are included.  
215 For surface networks with hourly data, e.g. NCDC, the observational data are paired up with the  
216 simulated data on an hourly basis for each site. The observational data and simulated data are  
217 averaged out for each site. The statistics are then calculated based on the site-specific data pairs.  
218 The satellite-derived data are usually available on a monthly basis, and the simulated data are also  
219 averaged out on a monthly basis. The satellite-derived data are regridded to the same domain and  
220 number of grid cells similar to the simulated data. The time dimension is removed for the  
221 climatological evaluation, the statistics are based on a site-specific average or a grid cell average.  
222 The statistics are then calculated based on the paired satellite-derived vs. simulated grid cell values.  
223 The spatial and temporal analyses include spatial plots of MB over CONUS, spatial overlay plots  
224 of averaged simulated and observational data, monthly climatologically-averaged time series of  
225 major meteorological and chemical variables, annual average time series; probability distributions  
226 of major meteorological and chemical variables, and spatial plots of major aerosol and cloud  
227 variables compared with satellite data. A summary of the observational data from surface networks

228 and satellite retrievals can be found in Table S3. The variables that are analyzed in this study  
229 include O<sub>3</sub>, particulate matter with diameter less than and equal to 2.5 and 10 μm (PM<sub>2.5</sub> and PM<sub>10</sub>,  
230 respectively), and PM<sub>2.5</sub> species including sulfate (SO<sub>4</sub><sup>2-</sup>), ammonium (NH<sub>4</sub><sup>+</sup>), nitrate (NO<sub>3</sub><sup>-</sup>), EC,  
231 OC, and total carbon (TC = EC + OC), temperature at 2-m (T2), relative humidity at 2-m (RH2),  
232 and wind speed at 10-m (WS10), wind direction at 10-m (WD10), precipitation, aerosol optical  
233 depth (AOD), cloud fraction (CLDFRA), cloud water path (CWP), cloud optical thickness (COT),  
234 CDNC, cloud condensation nuclei (CCN), downward shortwave radiation (SWDOWN), net  
235 shortwave radiation (GSW), downward longwave radiation (GLW), outgoing longwave radiation  
236 at the top of atmosphere (OLR), and shortwave and longwave cloud forcing (SWCF and LWCF).  
237 While uncertainties exist in all the observational data used, systematic uncertainty  
238 analysis/quantification is beyond the scope of this work. In this work, all observational data are  
239 considered to be the true values in calculating the performance statistics. The information on the  
240 accuracy of most data used in the model evaluation has been provided in Table 2 of Zhang et al.  
241 (2012a). Uncertainties associated with some of the observational data are discussed in Section 3.

### 242 **3. Model Performance Evaluation**

#### 243 **3.1 Meteorological Predictions**

244 Table 2 summarizes the statistics for T2, RH2, WS10, WD10, and precipitation. The model  
245 performs very well for a 10-year average T2 with a slight underprediction (an MB of -0.3 °C).  
246 This is better or consistent with other studies which tend to report underpredictions in simulated  
247 T2. Brunner et al. (2014) reported a range of monthly MBs for T2 of -2 to 1 °C for simulations  
248 using a number of CTMs over individual years for 2006 and 2010 with reanalysis meteorological  
249 ICs/BCs. Seasonal temperature biases of -1.8 to -2.3 °C were reported from an ensemble of  
250 regional climate models (RCMs) for a simulation period of 1971 to 2000 over the Northeast

251 (Rawlins et al., 2012). He et al. (2015) also showed biases of -3 to 0°C over CONUS when  
252 compared against NCEP reanalysis data. Kim et al. (2013) compared the results of a number of  
253 RCMs over CONUS over a climatological period of 1980 to 2003 against Climatic Research Unit  
254 (CRU) surface analysis data at a 0.5° resolution and reported T2 biases of -5 to 5 °C. Figure 9.2  
255 from Flato et al. (2013) shows that the Coupled Model Intercomparison Project Phase 5 (CMIP5)  
256 models tend to underpredict T2 for the period of 1980 to 2005 over western U.S. by up to -3 °C.  
257 The slight bias in T2 can be attributed to errors in soil temperature and soil moisture (Pleim and  
258 Gilliam, 2009) or errors in the green vegetation fraction in the National Center for Environmental  
259 Prediction, Oregon State University, Air Force and Hydrologic Research Lab (NOAH) Land  
260 Surface Model (LSM) (Refslund et al., 2013). RH2 and WS10 are slightly overpredicted.  
261 Precipitation is largely overpredicted, consistent with overpredictions in precipitation from WRF  
262 and WRF/Chem simulations reported in literatures. For example, Caldwell et al. (2009) attributed  
263 the overprediction in precipitation to overprediction in precipitation intensity but underprediction  
264 in precipitation frequency. Otte et al. (2012) also reported that the precipitation predicted by WRF  
265 is too high compared to the North American Regional Reanalyses (NARR) data throughout the  
266 whole CONUS domain over a period of 1988 – 2007. Nudging and reinitialization have been most  
267 commonly used methods to control such errors. . Three sensitivity simulations are conducted for  
268 a summer month (July 2005) to pinpoint likely causes of the precipitation biases. The baseline  
269 simulation (**Base**) uses a monthly reinitialization frequency, CESM\_NCSU ICs/BCs, and the Grell  
270 3D cumulus parameterization. The sensitivity simulations include (1) **Sen1**, which is similar to the  
271 Base case except with a 5-day reinitialization period; (2) **Sen2**, which is similar to Base except  
272 using NCEP for the meteorological ICs/BCs; and (3) **Sen3**, which is similar to Base except using  
273 WRF/Chem v3.7 with the Multi-Scale Kain Fritsch (MSKF) cumulus parameterization, instead

274 of Grell 3D. The differences in configuration setup in those sensitivity simulations are given in  
275 Table S4. The evaluation and comparison of the baseline and sensitivity results in July 2005 are  
276 summarized in Tables S5 and S6, and Figure S1 in the supplementary material. As shown in Tables  
277 S5-S6 and Figure S1, the precipitation bias can be attributed to several factors including the use of  
278 Grell 3D cumulus parameterization scheme, the use of bias-corrected CESM\_NCSU data (instead  
279 of NCEP reanalysis data), and the use of an reinitialization frequency of 1-month, among which  
280 the first factor dominates the biases in precipitation predictions. The simulated precipitation is  
281 very sensitivity to different cumulus parameterizations. Compared to scale-aware  
282 parameterizations such as the multi-scale Kain-Fritsch (MSKF) cumulus scheme, the Grell 3D  
283 parameterization has a tendency to overpredict precipitation, particularly over ocean.

284 Figure 1 shows the spatial distributions of MB for 10-year average predictions of T2, RH2,  
285 WS10, and precipitation. Figure 2 shows the time series of 10-year average monthly and annual  
286 average T2, WS10, RH2, precipitation, O<sub>3</sub>, and PM<sub>2.5</sub> against observational data and IOA statistics.  
287 T2 (Figure 1a) tends to be underpredicted over eastern and western U.S. and overpredicted over  
288 the central U.S. The bias correction method itself may also contribute to the slight biases in T2. A  
289 single temporally averaged (2001 – 2010) NCEP reanalysis file is applied to the 6-hourly BCs for  
290 each individual year, which would in some cases contribute to the biases in the climatological 10-  
291 year evaluation. T2 also tends to be underpredicted during the cooler months but overpredicted  
292 during the warmer months (Figure 2a). While the bar charts in Figure 2 show domain- average  
293 mean observed and mean simulated T2, IOA performance takes into account the proportion of  
294 differences between mean observed and mean simulated values at different sites. IOA can be  
295 calculated as,

296

$$IOA = 1 - \frac{\sum_i^N (O_i - S_i)^2}{\sum_i^N (|O_i - \bar{O}| + |S_i - \bar{S}|)^2} \quad (2)$$

297 where  $O_i$  and  $S_i$  denote time-dependent observations and predictions at time and location  $i$ ,  
 298 respectively,  $N$  is the number of samples (by time and/or location),  $\bar{O}$  denotes mean observation  
 299 and  $\bar{S}$  denotes mean predictions over all time and locations, they can be calculated as:

300

$$\bar{O} = (1/N) \sum_{i=1}^N O_i, \quad \bar{S} = (1/N) \sum_{i=1}^N S_i,$$

301 IOA values range from 0-1, with a value of 1 indicating a perfect agreement.

302 The model performance in terms of IOA for T2 is slightly worse during the warmer months  
 303 as compared to the cooler months; however, IOA values for all months are  $\geq 0.9$ . The poorer IOA  
 304 statistics for the warmer months are possibly influenced to a certain extent by the fact that the IOA  
 305 tends to be more sensitive towards extreme values (when temperatures are maximum) due to the  
 306 squared differences used in calculating IOA (Legates and McCabe, 1999). As shown in Figures 1b  
 307 and 2b, the spatial distributions of MBs for RH2 follow closely the spatial distributions of MBs  
 308 for T2, where T2 is underpredicted, RH2 is overpredicted and vice versa. Unlike T2, the IOA for  
 309 RH2 is the highest during the warmer months and the lowest during the winter months, but IOA  
 310 for RH2 is generally high ( $> 0.7$ ) for all months. WS10 is also generally overpredicted along the  
 311 coast, over eastern U.S. and some portions over the western U.S. (Figure 1c), consistent with  
 312 overpredictions of T2 over the coast, and partially due to unresolved topographical features. In this  
 313 case the topographic correction for surface winds used to represent extra drag from sub-grid  
 314 topography (Jimenez and Dudhia, 2012) is used as an option in the 10-yr WRF/Chem simulations;  
 315 however, WS10 is still overpredicted except for the areas of flat undulating land in the central U.S.  
 316 Jimenez and Dudhia (2012) also suggested that the grid points nearest to the observational data

317 might not be the most appropriate or most representative, and that the selection of nearby grid  
318 points can help to reduce errors in surface wind speed estimations. In this study, as the evaluation  
319 is conducted over the whole CONUS, the nearest grid points are used for evaluation, which could  
320 also result in errors in wind speed evaluation. The positive T2 and WS10 bias along the coast could  
321 be due to the fact that the model grids for temperatures and wind speeds are located over the ocean,  
322 however, the observation points are located slightly inland. As shown in Figure 2, WS10 performs  
323 well on average for the months of April, May, and June, and is overpredicted for the other months.  
324 Nonetheless the climatological NMB for WS10 overall is low at 7.7% (Table 2). WS10 has higher  
325 IOA values during the spring months and the lowest IOA during the summer months and in  
326 November. The model performs relatively well in predicting WD10 variability with a Corr of 0.6,  
327 indicating overall a more southerly direction domain-wide predicted by the model compared to  
328 observations. Precipitation is overpredicted for all months except for June, especially during the  
329 summer months of July to August. Even with the inclusion of radiative feedback effects from the  
330 subgrid-scale clouds in the radiation calculations, precipitation is still overpredicted with the Grell  
331 3D scheme, which is consistent with the results shown by Alapaty et al. (2012). Precipitation  
332 mainly has lower IOAs during the summer compared to other months, except in June which  
333 actually exhibits the largest IOA of all months. Even though June is considered a summer month,  
334 it does not show overprediction in precipitation compared to the other summer months. It is  
335 possible that in June, the overall atmospheric moisture content is low. This is consistent with  
336 simulated RH2 as June is the only month where RH2 is underpredicted compared to observations.

337 In general the model is able to reproduce the monthly trends in meteorological variables;  
338 for example, the predicted trend in T2 closely follows the observed trends by the [National Climatic](#)  
339 [Data Center](#) (NCDC). The observed RH2 decreases from January to a minimum in April, and then

340 increases from April to December. Although the model predicts a similar pattern in RH2, there is  
341 a lag in the RH2 minimum occurring two months later in June (Figure 2b). For WS10, the  
342 observation peaks in April, as compared to the simulated peak in March. The model correctly  
343 predicts the observed WS10 minimum occurring in August. The model trend in precipitation is  
344 similar to observations, except during the summer months of July through September, where a  
345 large overprediction leads to a sharp increase in July, followed by a gradual decrease through  
346 December.

347         Figures 2e – 2h show the annual time series trends for T2, RH2, WS10, and precipitation.  
348 The model performs relatively well in predicting the annual mean T2 for most years (with MBs of  
349  $< 0.5$  °C; Figure 2e). T2 also does not show an obvious decreasing or increasing T2 trend between  
350 2001 and 2010. The IOA for annual T2 for all years are  $> 0.95$ . However for 2002, mean simulated  
351 T2 is  $\sim 0.7$  °C higher than the observational data. IOA is still high for 2002 which indicates  
352 probably good performance of T2 at most sites, however with large overpredictions at a few sites  
353 which could skew the mean observed and mean simulated value but not influence IOA  
354 significantly. RH2 is consistently overpredicted by the model with the largest overprediction in  
355 2009. With the exception of 2009, observed RH2 is rather steady (65 – 70 %) from 2001 to 2010.  
356 IOA is also steady for RH2, except for 2009. As mentioned earlier, WRF tends to overpredict  
357 WS10 in general. Figure 2g shows that observations indicate weaker wind speeds from 2001 to  
358 2007. Model performance is better from 2007 to 2010 with higher IOAs compared to previous  
359 years. WRF has worse performance especially at weaker wind speeds as is the case from 2001 to  
360 2007. Model performance for precipitation is more variable year-to-year, with IOAs ranging from  
361 0.4 to 0.7; however, there is a systematic positive bias during the 10 year period.

362 Figure 3 shows the probability distributions of T2, RH2, WS10, and precipitation against  
363 NCDC and NADP for 10 years. The observed and simulated variables are averaged at each site  
364 for the 10-year period, and the pairs are then distributed into a probability distribution over 30 bins  
365 of observed and simulated values of T2. For T2, the simulated and observed probability  
366 distributions are very similar (Figure 3a), consistent with the statistics for T2 which shows only a  
367 small cold bias. The model overpredicts T2 at sites where temperatures are very low. The  
368 probability distribution curve for simulated RH2 is also shifted to the right of the observed RH2  
369 (Figure 3b), with an observed and modeled peak 74% and 78% respectively. The probability  
370 distribution of simulated WS10 is narrower (between 2 and 6 m s<sup>-1</sup>) compared to that of observed  
371 WS10 (between 1 and 7 m s<sup>-1</sup>). The model thus overpredicts when near-surface wind speeds are  
372 low, but underpredicts when wind speeds are very high. This suggests that the surface drag  
373 parameterization is still insufficient to help predict low wind speeds; however, it might have  
374 contributed to the reduction in the simulated high wind speeds (Mass, 2012). The probability  
375 distribution for simulated precipitation against NADP also shows a shift to the right, consistent  
376 with the statistics for overpredicted precipitation and also with the probability curve of RH2.  
377 Nasrollahi et al. (2012) examined 20 combinations of microphysics and cumulus parameterization  
378 schemes available in WRF and found that most parameterization schemes overestimate the amount  
379 of rainfall and the extent of high rainfall values. In this study, while Grell 3D Ensemble cumulus  
380 parameterization contributes in part to the overpredictions of precipitation, most overpredictions  
381 occur at high thresholds as shown in Figure 3 (d) and they are attributed to possible errors in the  
382 Morrison two moment scheme because the overpredictions of non-convective precipitation  
383 dominate the overpredictions of total precipitation.

### 384 **3.2 Chemical Predictions**

### 385 3.2.1 Ozone

386 Table 2 summarizes the statistics for major chemical species. The model overpredicts  
387 hourly O<sub>3</sub> mixing ratios on average against the Aerometric Information Retrieval System (AIRS)  
388 – Air Quality System (AQS) with an NMB of 9.7% and an NME of 22.4%, but underpredicts O<sub>3</sub>  
389 mixing ratios against the Clean Air Status and Trends Network (CASTNET) with an NMB of -  
390 8.8% and an NME of 19.8%. The O<sub>3</sub> mixing ratios are overpredicted at AIRS-AQS sites for all  
391 climatological months except for April and May (Figure 4a) but underpredicted at CASTNET sites  
392 for all months except for October with the largest underpredictions occurring in April and May  
393 where IOA statistics are the lowest (Figure 4b). IOA statistics for all climatological months range  
394 from 0.5 to 0.6 for AIRS-AQS and from 0.4 to 0.9 for CASTNET. In general, IOA values tend to  
395 be higher for CASTNET compared to AIRS-AQS during the fall and winter months of October to  
396 March. The IOA values for AIRS-AQS are rather steady on average over the 12 months compared  
397 to CASTNET. This can be attributed to the larger dataset of AIRS-AQS (> 1000 stations)  
398 compared to CASTNET (< 100 stations), the high and low undulations in O<sub>3</sub> averages at the  
399 CASTNET sites tend to be smoothed or averaged out in O<sub>3</sub> averages at the AIRS-AQS sites given  
400 larger AIRS-AQS dataset. The observed data from AIRS-AQS and CASTNET also show the  
401 highest monthly O<sub>3</sub> mixing ratios over April and May. This result is consistent with the findings  
402 of Cooper et al. (2014), who reported the highest mass of tropospheric O<sub>3</sub> for the northern  
403 hemisphere in April and May based on the Ozone Monitoring Instrument (OMI) measurements in  
404 2004, which suggested that the column mass of O<sub>3</sub> is not necessarily proportional to nitrogen oxide  
405 (NO<sub>x</sub>) emissions that peak during the summer. In addition, Cooper et al. (2014) attributed a shift  
406 in the seasonal O<sub>3</sub> cycle observed at many rural mid-latitude monitoring sites to emissions  
407 reductions in the U.S. The same study also reported that the summertime O<sub>3</sub> mixing ratios were

408 lower in eastern U.S. between 2005 and 2010 when compared to previous years, while remaining  
409 relatively constant in spring. Thus the summer O<sub>3</sub> maximum during 2001- 2004 was replaced by  
410 a broad spring/summer peak in 2005 - 2010. Both the observed and simulated O<sub>3</sub> mixing ratios do  
411 not decrease for AIRS-AQS and CASTNET from 2001 to 2010 (Figures 4e and 4f). This is  
412 somewhat consistent with Cooper et al. (2014) which showed that surface and lower tropospheric  
413 O<sub>3</sub> has a decreasing trend over eastern U.S. but an increasing trend over the western U.S. from  
414 1990-1999 to 2010. The predicted annual average O<sub>3</sub> mixing ratios are consistent from 2001 to  
415 2010, with overpredictions and IOAs of ~0.6 at the AIRS-AQS sites, and underpredictions and  
416 IOAs of ~0.6 to 0.8 at the CASTNET sites.

417 Figure 5 shows the probability distributions of maximum 1-hour and 8-hour O<sub>3</sub> mixing  
418 ratios against CASTNET and AIRS-AQS. The probability distributions of the observed and  
419 simulated O<sub>3</sub> mixing ratios are very similar. The model is able to simulate the range and  
420 probabilities of O<sub>3</sub> mixing ratios relatively well at both CASTNET and AIRS-AQS sites. At the  
421 CASTNET sites as shown in Figures 5a and b, the model accurately predicts the peak maximum  
422 1-hour O<sub>3</sub> mixing ratio centered at ~60 ppb, however, slightly underpredicts the peak maximum  
423 8-hour O<sub>3</sub> mixing ratio by a few ppb. At the AIRS-AQS sites as shown in Figures 5c and d, the  
424 predicted probability distribution curve is slightly shifted to the right of the observations for both  
425 maximum 1-hour and 8-hour O<sub>3</sub> mixing ratios. It is also interesting to note that the probability  
426 distributions for CASTNET and AIRS-AQS are quite different. O<sub>3</sub> at the AIRS-AQS sites has a  
427 unimodal normal distribution, while O<sub>3</sub> at the CASTNET sites has a bi-modal distribution, with a  
428 tail of the distribution extending toward lower O<sub>3</sub> mixing ratios (0 – 20 ppb). The peak distribution  
429 occurs at around 10 ppb, because the O<sub>3</sub> mixing ratios are low at most CASTNET sites. The  
430 second peak at ~60 ppb for CASTNET occurs mainly around the summer months during which

431 O<sub>3</sub> is produced through photochemistry involving its precursors. These distributions are attributed  
432 to the nature of the sites' locations, where the AIRS-AQS network includes a mixture of urban,  
433 suburban and rural sites, leading to a normal distribution of O<sub>3</sub> mixing ratios centered at relatively  
434 higher O<sub>3</sub> mixing ratios, while the CASTNET network includes mostly rural sites that exhibit a  
435 low maximum 1-hour and 8-hour O<sub>3</sub> mixing ratios, thus leading to a distribution with a tail skewed  
436 towards the lower O<sub>3</sub> mixing ratios.

437 Figure 6 shows the diurnal variation of O<sub>3</sub> concentrations and IOA statistics for the four  
438 climatological seasons against CASTNET (Figures a to d) and AIRS-AQS (Figures e to h) (Winter  
439 - January, February and December (JFD); Spring - March, April, and May (MAM); Summer -  
440 June, July, and August (JJA); Fall - September, October, and November (SON). Figure 6a shows  
441 that in more rural sites (CASTNET) in winter O<sub>3</sub> tends to be underpredicted during the morning  
442 (01:00 – 09:00 local standard time (LST)) and evening hours (18:00 – 24:00 LST). However,  
443 Figure 6b shows that in general for all AIRS-AQS sites including urban sites, O<sub>3</sub> is systematically  
444 overpredicted for all hours of the day. The diurnal trends for CASTNET and AIRS-AQS are  
445 completely opposite for winter. As CASTNET sites are located in areas where urban influences  
446 are minimal, most of these sites are likely to be NO<sub>x</sub>-limited sites (Campbell et al., 2014).  
447 Underpredicted NO<sub>x</sub> emissions in rural areas can lead to underpredictions in O<sub>3</sub> concentrations in  
448 NO<sub>x</sub>-limited areas. As shown in Figure 2a), T2 is generally overpredicted during the winter  
449 months, which explains the overpredictions in O<sub>3</sub> for most sites against AIRS-AQS. As shown in  
450 Figures 6a, b and c, for CASTNET, the diurnal variations of O<sub>3</sub> in MAM and JJA are similar to  
451 that in JFD. As shown in Figure 6d, slight overpredictions during the daylight hours of 10:00 to  
452 17:00 LST occur in SON at the CASTNET sites, however the trends are similar for morning and  
453 evening hours as compared to the other seasons. Similar to SON at the CASTNET sites, for AIRS-

454 AQS sites, overpredictions during daylight hours occur in JJA and SON (Figures 6 g and h), and  
455 also to a much lesser extent in MAM (Figure 6f). This is probably due to the overpredictions of  
456 T2, which are the smallest during MAM compared to other months as shown in Figure 2a.

457 Figure 7 compares the spatial distributions of 10-year average of the predicted and  
458 observed hourly O<sub>3</sub> mixing ratios. The O<sub>3</sub> mixing ratios tend to be underpredicted in eastern and  
459 northeastern U.S., where most of the CASTNET sites are located (Figure 7a). This is consistent  
460 with the diurnal trends from Figures 6a to d which also show underpredictions for CASTNET sites.  
461 From Figure 1a, T2 is underpredicted on average over northeastern U.S., which results in  
462 underpredictions in biogenic emissions in the rural areas from MEGAN2. This would in turn  
463 reduce O<sub>3</sub> mixing ratios in VOC-limited areas. O<sub>3</sub> photochemical reactivities would also be  
464 reduced due to reduced T2. O<sub>3</sub> mixing ratios are, however, overpredicted over northwestern U.S.,  
465 and also near the coastline of western U.S. The overprediction of O<sub>3</sub> mixing ratios in northwestern  
466 U.S. can be attributed to an overprediction in the chemical BCs from CESM, as indicated by the  
467 high O<sub>3</sub> mixing ratios near the northwestern region of the domain boundary.

### 468 **3.2.2 Particulate Matter**

469 The 10-year average PM<sub>2.5</sub> concentrations are overpredicted with an NMB of 23.3 %  
470 against IMPROVE, and underpredicted with an NMB of -10.8 % against the Speciated Trends  
471 Network (STN) (Table 2). In addition, the IOA trend in Figure 4c shows very good performance  
472 for PM<sub>2.5</sub> against the Interagency Monitoring of Protected Visual Environments (IMPROVE) with  
473 IOA values > 0.8. IOA values for PM<sub>2.5</sub> against STN are high (~ 0.6 – 0.8) during the spring and  
474 summer months, but lower (~ 0.4) during the winter months (Figure 4d). The IMPROVE surface  
475 network covers generally rural areas and national parks while the STN surface network covers  
476 urban sites. The horizontal resolution of 36×36 km<sup>2</sup> used in this study may be too coarse to resolve

477 the locally high PM<sub>2.5</sub> concentrations at urban sites in STN which are in proximity of significant  
478 point sources, especially during the fall and winter. During these colder seasons, PM<sub>2.5</sub>  
479 concentrations over the U.S. in general tend to be higher due to an extensive use of woodstove and  
480 cold temperature inversions, which trap particulates near the ground (EPA, 2011). As shown in  
481 Table 2, the concentrations of PM<sub>2.5</sub> species such as SO<sub>4</sub><sup>2-</sup>, OC, and TC are overpredicted at the  
482 IMPROVE sites, while the concentrations of the other main PM<sub>2.5</sub> species NO<sub>3</sub><sup>-</sup>, NH<sub>4</sub><sup>+</sup>, and EC are  
483 underpredicted at both IMPROVE and STN sites. TC concentrations, which are the sum of OC  
484 and EC, are overpredicted due to larger overpredictions of OC compared to the underpredictions  
485 of EC. The model also simulates both primary organic aerosol (POA) and secondary organic  
486 aerosol (SOA). OC is calculated as the sum of POA and SOA divided by the ratio of OA/OC,  
487 which is assumed to be a constant of 1.4 (Aitken et al., 2008). This calculation of OC using a  
488 constant of 1.4 is an approximation, which is subject to uncertainties when comparing simulated  
489 OC against observational data, as the ratio of OA/OC can be different in different environments  
490 (Aitken et al., 2008).

491 As shown in Table 2, at the STN sites, the model slightly overpredicts the concentrations  
492 of SO<sub>4</sub><sup>2-</sup>, while underpredicting those of NO<sub>3</sub><sup>-</sup>, NH<sub>4</sub><sup>+</sup>, and EC. The overpredictions of SO<sub>4</sub><sup>2-</sup> are  
493 likely due to the uncertainties that arise from processing of the RCP SO<sub>2</sub> emissions. The RCP SO<sub>2</sub>  
494 emissions are only available as a total emission flux, and they are not vertically distributed to the  
495 important point sources such as furnaces and stacks. In this work, two steps are taken to resolve  
496 the RCP elevated SO<sub>2</sub> emissions in each emission layer. First, a set of factors are derived from the  
497 fraction of the elevated emissions in each layer to the vertical sum of emissions for NEI used by  
498 default in the SMOKE model with the NEI data. Second, these factors are applied to the total RCP  
499 emissions to obtain SO<sub>2</sub> emissions in each emission layer. The total RCP SO<sub>2</sub> emissions were

500 higher than the total NEI emissions, resulting in higher surface and elevated SO<sub>2</sub> emissions.  
501 Figures 4g and 4h compare the modeled annual average time series for PM<sub>2.5</sub> against IMPROVE  
502 and STN observations, respectively. In general, the model performs well for PM<sub>2.5</sub> at the  
503 IMPROVE (IOA > 0.8) and STN (IOA ~ 0.5 – 0.7) sites. A declining trend in PM<sub>2.5</sub> observed and  
504 simulated concentrations are also observed over the years. For the later years (2007 to 2010), the  
505 model performs significantly better against IMPROVE compared to STN. As 2010 NEI emissions  
506 are used for the years 2007 to 2010, there are not many variations in the simulated PM<sub>2.5</sub>  
507 concentrations over these 4 years.

508         Figures 7 and 8 show the spatial plots of 10-yr average of simulated 24-hour average ,  
509 PM<sub>10</sub>, PM<sub>2.5</sub>, and PM<sub>2.5</sub> species concentrations, overlaid with observations from both STN and  
510 IMPROVE. The underpredictions of PM<sub>10</sub> are dominated by an underprediction in the wind-blown  
511 dust emissions, especially in western U.S. (Figure 7b). This is confirmed in Table 2, which shows  
512 an MB of -11.5 µg m<sup>-3</sup> and an NMB of -51.2% against PM<sub>10</sub> observations at AIRS-AQS sites. The  
513 observational data indicate the elevated concentrations of dust over portions of Arizona and  
514 California (> 50 µg m<sup>-3</sup>), which are not reproduced by the simulations (the simulated  
515 concentrations are much lower, < 20 µg m<sup>-3</sup>). The AER/AFWA dust module (Table 1) does not  
516 produce sufficient dust in this case, even though WS10 is overpredicted and is proportional to the  
517 dust emissions. The sea-salt emission module by Gong et al. (1997), however, seems to produce a  
518 reasonable amount of sea-salt as shown by the similar concentrations between simulated and  
519 observational data for PM<sub>10</sub> near the coastlines. In addition, the MADE/VBS module in  
520 WRF/Chem does not explicitly simulate the formation/volatilization of coarse inorganic species.  
521 The coarse inorganic species are available, however, in the emissions and are transported and  
522 deposited in a manner that is similar to non-reactive tracers.

523 The model performs well for PM<sub>2.5</sub> over eastern U.S. (Figure 7c), where modeled  
524 concentrations are close to the observations; however, over the western U.S. there are  
525 underpredictions in PM<sub>2.5</sub>, especially in central to southern California. Even though Table 2 shows  
526 in general an overprediction of SO<sub>4</sub><sup>2-</sup> against STN sites, the model underpredicts SO<sub>4</sub><sup>2-</sup> in regions  
527 of elevated SO<sub>4</sub><sup>2-</sup> concentrations, in particular, where concentrations are above 10 μg m<sup>-3</sup> in the  
528 vicinity of significant point sources of SO<sub>2</sub> and SO<sub>4</sub><sup>2-</sup> over eastern U.S. (Figure 7d). This is likely  
529 due to the coarse resolution (0.5° × 0.5°) of RCP emissions, which probably results in a general  
530 overprediction of SO<sub>2</sub> emissions over a grid but cannot resolve point sources smaller than the grid  
531 resolution. A similar pattern is found for NH<sub>4</sub><sup>+</sup> over eastern U.S. due to underpredictions of high  
532 concentrations of SO<sub>4</sub><sup>2-</sup> (Figure 8a). There are also large underpredictions in NH<sub>4</sub><sup>+</sup> over the western  
533 U.S. The underpredictions in NH<sub>4</sub><sup>+</sup> are likely due to underpredictions of NH<sub>3</sub> emissions from RCP.  
534 The NH<sub>3</sub> emissions from RCP are much lower than those of NEI emissions over western U.S., by  
535 more than a factor of 5, especially over portions of California. Large underpredictions occur over  
536 both eastern and western U.S. for NO<sub>3</sub><sup>-</sup>, EC, and TC (Figures 8b, c, and d). The underpredictions  
537 in NO<sub>3</sub><sup>-</sup> are more likely influenced by the underpredictions of NH<sub>4</sub><sup>+</sup> rather than NO<sub>x</sub> emissions.  
538 NO<sub>x</sub> emissions for NEI are higher than those of RCP for a number of point sources, however, in  
539 general RCP has higher NO<sub>x</sub> emissions. Other possible reasons for the underpredictions of NO<sub>3</sub><sup>-</sup>  
540 concentrations include both prediction and measurement errors associated with SO<sub>4</sub><sup>2-</sup> and TNH<sub>4</sub>  
541 that can greatly affect the performance of NO<sub>3</sub><sup>-</sup>, inaccuracies in the assumptions used in the  
542 thermodynamic model (e.g., the assumption that inorganic ions are internally mixed and the  
543 equilibrium assumption might not be representative, especially for particles with larger diameters),  
544 as well as inaccuracies in T2 and RH predictions (Yu et al., 2005). The statistics for IMPROVE  
545 TC indicate overpredictions; however the statistics for STN TC indicate larger underpredictions

546 with an MB of  $-2.0 \mu\text{g m}^{-3}$ , which would explain the large underpredictions in  $\text{PM}_{2.5}$  concentrations  
547 over western U.S. The large underpredictions are in part impacted by uncertainties in emissions as  
548 well as due to uncertainties in the precursor gas emissions for these species, especially for TC. The  
549 RCP emissions of EC and POA are lower when compared to those of NEI. NEI emissions have a  
550 higher spatial resolution, and thus more adequately represent the emissions from point sources  
551 compared to RCP. The underpredictions of TC are also more likely due to underpredictions in EC  
552 as compared to OC, as shown in underpredictions of EC by Figure 8c. As T2 is slightly  
553 underpredicted, these could have resulted in underpredictions in isoprene and terpene, which are  
554 major gas precursors of biogenic SOA, resulting in lower SOA and OC concentrations. In addition,  
555 the emissions of anthropogenic VOC species from RCP which are also of a lower spatial resolution  
556 compared to their emissions in the NEI tend to also be lower than NEI levels especially at point  
557 sources. The underpredictions for these particulate species, especially for water-soluble species  
558 including  $\text{NH}_4^+$  and  $\text{NO}_3^-$  are also likely impacted by overpredictions in precipitation (Figure 2d),  
559 which leads to an overprediction in their wet deposition rates and thus a reduction of their ambient  
560 concentrations. The overpredictions in WS10 also help contribute to the deposition of  $\text{PM}_{2.5}$  and  
561  $\text{PM}_{2.5}$  species onto the ground (Sievering et al., 1987).

### 562 **3.3 Aerosol, Cloud, and Radiation Predictions**

563 There are uncertainties in the satellite retrievals of various aerosol-cloud-radiation  
564 variables from the Clouds and the Earth's Radiant Energy System (CERES) and the Moderate  
565 Resolution Imaging Spectroradiometer (MODIS). Loeb et al. (2009) reported that the major  
566 uncertainties of the top of atmosphere radiative fluxes from CERES are derived from instrument  
567 calibration (with a net error of  $4.2 \text{ W m}^{-2}$ ), and the assumed value of  $1 \text{ W m}^{-2}$  for total solar  
568 irradiance. However, there is good correlation ( $R > 0.8$ ) between the model and CERES for the

569 radiation variables SWDOWN, GSW, and GLW, which are all measured at the surface (Table 2).  
570 Modeled OLR at the top of the atmosphere also has relatively good correlation ( $R \sim 0.6$ ).  
571 SWDOWN and GLW are both slightly overpredicted due to influences from biases in PM  
572 concentrations and clouds, but GSW and OLR are slightly underpredicted.

573         The overpredictions of the surface radiation variables are also impacted by the  
574 underpredictions in AOD and COT. AOD is underpredicted with an NMB of -24.0%, and COT is  
575 underpredicted with an NMB of -44.3%. These underpredictions indicate that less radiation is  
576 attenuated (i.e., absorbed or scattered) or reflected while traversing through the atmospheric  
577 column and clouds, thus allowing more radiation to reach the ground. Using the CESM model, He  
578 et al. (2015) also showed underpredictions in AOD and COT over CONUS against MODIS  
579 satellite retrievals. Figure 9 compares the spatial distributions of the 10-year average predictions  
580 of AOD (a and b) against the satellite retrieval data from MODIS. The simulated AODs show  
581 relatively large values over eastern U.S., due to the relatively higher PM concentrations in this  
582 region of the U.S. The MODIS AOD, however, shows slightly elevated values over eastern U.S.,  
583 but the magnitudes are not as high as the simulated AOD over eastern U.S. MODIS-derived AOD  
584 is also higher over western U.S. compared to eastern U.S., and this trend is not found in the  
585 simulated AOD. The differences between the MODIS AOD and the simulated AOD are likely due  
586 to the differences in the algorithms used to retrieve AOD based on MODIS measurements and  
587 calculate AOD in WRF/Chem. For MODIS, AOD is calculated by matching the spectral  
588 reflectance observations with a lookup table based on a set of aerosol parameters including the  
589 aerosol size distributions from a variety of aerosol models, which differ based on seasons and  
590 locations (Levy et al., 2007). There are also different algorithms for dark land, bright land, and  
591 over oceans (Levy et al., 2013). The MODIS data are aggregated into a global  $1^\circ$  gridded (Level-

592 3) dataset with monthly (MOD08\_M3) temporal resolution  
593 ([https://www.earthsystemcog.org/site\\_media/projects/obs4mips/TechNote\\_MODIS\\_L3\\_C5\\_Aer](https://www.earthsystemcog.org/site_media/projects/obs4mips/TechNote_MODIS_L3_C5_Aerosols.pdf)  
594 [osols.pdf](https://www.earthsystemcog.org/site_media/projects/obs4mips/TechNote_MODIS_L3_C5_Aerosols.pdf)). The inaccuracies for the calculation of AOD in WRF/Chem include biases in aerosol  
595 size distribution, aerosol composition, aerosol water content, and reflectances. They can also arise  
596 from parameterizations in the calculations including the assumption of an internally-mixed aerosol  
597 composition. Therefore, caution should also be taken when comparing simulated AOD with the  
598 satellite-derived AOD products. Toth et al. (2013) compared Aqua MODIS AOD products over  
599 the mid to high latitude Southern Ocean where a band of enhanced AOD is observed, to cloud and  
600 aerosol products produced by the Cloud-Aerosol Lidar with Orthogonal Polarization (CALIOP)  
601 project; and AOD data from the Aerosol Robotic Network (AERONET) and the Maritime Aerosol  
602 Network (MAN). They concluded that the band of enhanced AOD is not detected in the CALIOP,  
603 AERONET, or MAN products. The enhanced AOD band is attributed to stratocumulus and low  
604 broken cumulus cloud contamination, as well as the misidentification of relatively warm cloud  
605 tops compared with surrounding open seas.

606 Figure 9 also shows spatial distributions of the 10-year average predictions of CDNC (c  
607 and d), CWP (e and f), and COT (g and h), compared against the satellite retrieval data from  
608 MODIS. The cloud variables CDNC, CWP, and COT tend to be underpredicted for most of the  
609 regions over the U.S. However, CWP is largely overpredicted over the Atlantic ocean. This is also  
610 likely due to the build-up of moisture over the Atlantic ocean, also influencing precipitation as  
611 mentioned previously. CDNC is overpredicted over some regions in eastern U.S., but there are  
612 also relatively large areas of underpredictions over both the land and ocean. This leads to an  
613 average domain-wide underprediction for CDNC (Table 2). This is likely due to the differences in  
614 deriving CDNC in the model and in the satellite retrievals. CDNC in the model is calculated based

615 on the activation parameterization by Abdul Razzak and Ghan (2000) based on the aerosol size  
616 distribution, aerosol composition, and the updraft velocity. The MODIS-derived CDNC from  
617 Bennartz (2007) is calculated based on cloud effective radius and COT, which would explain the  
618 differences in spatial patterns between model and observed data. As indicated by Bennartz (2007),  
619 the errors in CDNC can be up to 260%, especially for regions with low CF ( $< 0.1$ ). The model and  
620 MODIS spatial patterns are similar for CWP and COT over land, although the model values are  
621 underpredicted. King et al. (2013) reported that the MODIS retrieval of cloud effective radius  
622 when compared to in-situ observations is overestimated by 13% on average. Combined with  
623 overestimations in COT, this leads to overestimation of liquid water path. In addition, there can  
624 also be differences in satellite-derived cloud products from different satellites. For example, Shan  
625 et al. (2011) showed that the derived CLDFRA from MODIS and another satellite, the Polarization  
626 and Directionality of Earth Reflectances (POLDER) can differ with a global average of 10%.

627         Figure 10 shows similar spatial plots for modeled versus CERES derived SWDOWN,  
628 OLR, SWCF, and LWCF. We note that modeled SWCF is calculated based on the differences  
629 between the net cloudy sky and net clear sky shortwave radiation at the top of atmosphere, which  
630 in turn are dependent on cloud properties including the CLDFRA, COT, cloud asymmetry  
631 parameter, and cloud albedo. It is possible that due to the overprediction of CLDFRA, the  
632 magnitudes of the simulated SWCF are greater than those from CERES (Figures 10c and 10g),  
633 even though the other cloud variables are underpredicted. LWCF is calculated based on the  
634 differences in clear-sky OLR and cloudy-sky OLR, which in turn are dependent on CLDFRA,  
635 COT, and absorbance and radiance due to atmospheric gases. The underprediction of total-sky  
636 OLR (Table 2 and Figures 10b and 10f) leads to an overprediction in LWCF. SWCF is largely  
637 overpredicted over eastern U.S. and especially over the Atlantic ocean (Figures 10c and 10g).

638 LWCF is also overpredicted by the model in similar locations as SWCF, such as in southeastern  
639 U.S., and over the ocean in the eastern portion of the domain (Figures 10d and 10h). This is further  
640 confirmed by the underpredictions in SWDOWN over the Atlantic ocean and in general over the  
641 eastern portion of the domain, as increased clouds (as a consequence of overpredicted AOD, CWP  
642 and COT) and SWCF lead to less SWDOWN reaching the ground (Figures 10a and 10e) which  
643 also eventually leads to a reduction in the OLR also over the eastern portion of the domain. The  
644 larger negative SWCF and positive LWCF in the model compared to CERES, however, lead to an  
645 overall good agreement with CERES for the net cloud forcing (SWCF + LWCF; not shown). The  
646 mean bias for SWCF against CERES of  $7.8 \text{ W m}^{-2}$  and that for LWCF against CERES of  $6.9 \text{ W}$   
647  $\text{m}^{-2}$  are comparable to the results from the CMIP5 models of  $-10$  to  $10 \text{ W m}^{-2}$  over CONUS region  
648 (Figure 9.5 in Flato et al., 2013). The evaluation of 10-year averaged predictions of aerosol-cloud-  
649 radiation variables is similar to the results from the WRF/Chem simulations in 2006 and 2010 by  
650 Yahya et al. (2014 and 2015). For example WRF/Chem generally performs well for cloud fraction  
651 but AOD, CDNC, CWP and COT are underpredicted in both studies, which possibly indicate  
652 consistent biases for every year contributing to climatological biases.

#### 653 **4. Summary and Conclusions**

654 Overall, the model slightly underpredicts T2 with a mean bias of  $\sim -0.3 \text{ }^\circ\text{C}$ , which is  
655 consistent or better than other studies based on chemical transport models and regional climate  
656 models. The underpredictions in T2 correlate to the overpredictions in RH2. WS10 biases are  
657 likely due to issues with unresolved topography or due to inaccuracies in the selection of  
658 representative grid points. There are seasonal biases in precipitation, where overpredictions tend  
659 to occur largely over the summer months; however, precipitation is overpredicted every year  
660 between 2001 and 2010 likely due mainly to uncertainties in WRF cumulus and microphysics

661 parameterizations. in particular, the use of a different cumulus parameterization scheme, e.g.,  
662 based on the MSKF available in WRF/Chem version 3.7 or newer has been shown in the sensitivity  
663 study to significantly reduce precipitation biases. Other factors contributing to the precipitation  
664 bias include the use of bias-corrected CESM\_NCSU data (instead of NCEP reanalysis data), and  
665 the use of an reinitialization frequency of 1-month. A satisfactory model performance for  
666 meteorological variables is important and necessary when simulating future years, as data  
667 evaluation is not possible. Meteorological variables such as temperature, humidity, wind speed  
668 and direction, PBL height, and radiation have a strong impact on chemical predictions, and thus  
669 are critical to the satisfactory model performance when predicting chemical variables such as O<sub>3</sub>  
670 and PM<sub>2.5</sub>. Biases in O<sub>3</sub> and PM<sub>2.5</sub> concentrations can be attributed to biases in any of the  
671 meteorological and chemical variables. The model performs generally well for radiation variables,  
672 as well as for the main chemical species such as O<sub>3</sub> and PM<sub>2.5</sub>, which indicates that the processed  
673 RCP 8.5 emissions are reasonably accurate to produce acceptable results for the concentrations of  
674 chemical species.

675 Modeled O<sub>3</sub> mixing ratios at the CASTNET sites are slightly underpredicted, but are  
676 slightly overpredicted at AIRS-AQS sites, in part due to the fact that the CASTNET sites are  
677 classified as rural, while the AIRS-AQS sites are classified as both urban and rural. O<sub>3</sub> mixing  
678 ratios at the AIRS-AQS sites tend to be overpredicted during the colder fall and winter seasons,  
679 and annually, O<sub>3</sub> mixing ratios are overpredicted every year from 2001 to 2010. O<sub>3</sub> mixing ratios  
680 at the CASTNET sites are underpredicted for all climatological months, while the largest  
681 underpredictions are observed from January to May. However, on a decadal time scale,  
682 WRF/Chem adequately represents the different O<sub>3</sub> probability distributions at the AIRS-AQS and  
683 CASTNET sites. This study also showed that peak O<sub>3</sub> mixing ratios are observed over April and

684 May rather than June to August, which is consistent with Cooper et al. (2014) who attributed this  
685 to emission reductions and opposite trends in O<sub>3</sub> mixing ratios over eastern and western U.S. over  
686 the last 20 years. Modeled PM<sub>2.5</sub> concentrations tend to be overpredicted at the IMPROVE sites  
687 but underpredicted at the STN sites. PM<sub>2.5</sub> at the IMPROVE sites tend to be underpredicted in  
688 spring and summer but overpredicted in fall and winter, while PM<sub>2.5</sub> concentrations against STN  
689 are persistently underpredicted for all climatological months. The IMPROVE and STN sites are  
690 classified as rural and urban, respectively. Due to the relatively coarse horizontal resolution of the  
691 model (36 × 36 km), the model is unable to capture the locally higher PM<sub>2.5</sub> concentrations at the  
692 STN sites. In general, however, the model performs relatively well for total PM<sub>2.5</sub> concentrations  
693 at the IMPROVE and STN sites with NMBs of within ±25%, although larger biases exist for PM<sub>2.5</sub>  
694 species. Model performance for PM<sub>10</sub> should be improved, as PM<sub>10</sub> also has important impacts on  
695 climate through influencing the radiative budget both directly and indirectly due to its larger size  
696 and higher concentrations. The choice of observational networks for model evaluation are  
697 therefore important as both networks can show positive and negative biases depending on the type  
698 and location of the sites (e.g., O<sub>3</sub> against AIRS-AQS and CASTNET, and PM<sub>2.5</sub> against STN and  
699 IMPROVE). The major uncertainties lie in the predictions of cloud-aerosol variables. As  
700 demonstrated in this study, large biases and error in simulating cloud variables even in the most  
701 advanced models such as WRF/Chem, indicating a need for future improvement in relevant model  
702 treatments such as cloud dynamics and thermodynamics, as well as aerosol-cloud interactions. In  
703 addition, there are large uncertainties in satellite retrievals of cloud variables for evaluation. In this  
704 study, most of the cloud-aerosol variables including AOD, COT, CWP, and CDNC are on average  
705 underpredicted across the domain; however, the overpredictions of cloud variables including COT  
706 and CWP over the Atlantic ocean and eastern U.S. lead to underpredictions in radiation and

707 overpredictions in cloud forcing, which are important parameters when simulating future climate  
708 change.

709 In summary, the model is able to predict O<sub>3</sub> mixing ratios and PM<sub>2.5</sub> concentrations  
710 relatively well with regards to decadal scale air quality and climate applications. The model is able  
711 to predict meteorological variables satisfactorily and with results comparable to RCM and GCM  
712 applications from literatures. Possible reasons behind the chemical and meteorological biases  
713 identified through this work should be taken into account when simulating longer climatological  
714 periods and/or future years. Aerosol-cloud-radiation variables are important for climate  
715 simulations, the performance of these variables are not as good as that of the chemical and  
716 meteorological variables. They contain consistent biases in single-year evaluations of WRF/Chem.  
717 However, magnitudes of biases for SWCF and LWCF are comparable to those from literature,  
718 which suggests that model improvements should be made in terms of bias correction of  
719 downscaled ICs/BCs as well as aerosol-cloud-radiation parameterizations in the model. In  
720 addition, having consistent physical and chemical mechanisms between the GCM and RCMs could  
721 help to reduce uncertainties in the results (Ma et al., 2014). Although CESM and WRF/Chem use  
722 similar chemistry and aerosol treatments in this work, they use somewhat different physics  
723 schemes which may contribute to such uncertainties. The development of scale-aware  
724 parameterizations that can be applied at both global and regional scales would help reduce  
725 uncertainties associated with the use of different schemes for global simulations and downscaled  
726 regional simulations.

## 727 **Acknowledgments**

728 This study is funded by the National Science Foundation EaSM program (AGS-1049200)  
729 at NCSU. For WRF/Chem simulations, we would like to acknowledge high-performance

730 computing support from Yellowstone (ark:/85065/d7wd3xhc) provided by NCAR's  
731 Computational and Information Systems Laboratory, sponsored by the National Science  
732 Foundation.

733

#### 734 **Code and Data Availability**

735 The WRF/Chem v3.6.1 code used in this paper will be available upon request. However,  
736 we highly encourage users to download the latest available version of the WRF/Chem code from  
737 NOAA's web site at [http://www2.mmm.ucar.edu/wrf/users/download/get\\_source.html](http://www2.mmm.ucar.edu/wrf/users/download/get_source.html). The  
738 updates in our in-house version of WRF/Chem v3.6.1 has been implemented into WRF/Chem  
739 v3.7 and WRF/Chem v3.7.1 for scientific community release. The WRF/Chem v3.7 and  
740 WRF/Chem v3.7.1 codes are now publicly available at

741 [http://www2.mmm.ucar.edu/wrf/users/download/get\\_source.html](http://www2.mmm.ucar.edu/wrf/users/download/get_source.html). These latest versions of the  
742 source codes contain all major changes in the standard version of WRF/Chem v3.6.1 used in for  
743 this study. In addition, they have been rigorously tested for compatibility and compiling issues  
744 on various platforms. The inputs including the meteorological files, meteorological initial and  
745 boundary conditions, chemical initial and boundary conditions, model set-up and configuration,  
746 and the namelist set-up, and instructions on how to run the simulations for a 1-day test case, as  
747 well as a sample output for 1-day test can be provided upon request.

748

#### 749 **References**

750 Abdul-Razzak, H. and Ghan, S. J.: A parameterization of aerosol activation, 2. Multiple aerosol  
751 types, *J. Geophys. Res.*, 105(5), 6837-6844, 2000.

752 Aitken, A.C., DeCarlo, P.F., Kroll, J.H., Worsnop, D.R., Huffman, J.A., Docherty, K.S., Ulbrich,  
753 I.M., Mohr, C., Kimmel, J.R., Sueper, D., Sun, Y., Zhang, Q., Trimborn, A., Northway, M.,  
754 Ziemann, P.J., Canagaratna, M.R., Onasch, T.B., Alfarra, M.R., Prevot, A.S.H., Dommen, J.,  
755 Duplissy, J., Metzger, A., Baltensperger, U. and Jimenez, J.L.: O/C and OM/OC ratios of  
756 primary, secondary and ambient organic aerosols with high-resolution time of flight aerosol  
757 mass spectrometry, *Environ. Sci. Technol.*, 42, 4478 – 4485, 2008.

758 Alapaty, K., Herwehe, J., Nolte, C.G., Bullock, R.O., Otte, T.L., Mallard, M.S., Dudhia, J. and  
759 Kain, J.S.: Introducing subgrid-scale cloud feedbacks to radiation in WRF, the 13<sup>th</sup> WRF Users  
760 Workshop, Boulder, CO, June 26 to 29, 2012.

761 Ahmadov, R., McKeen, S.A., Robinson, A.L., Bareini, R., Middlebrook, A.M., De Gouw, J.A.,  
762 Meagher, J., Hsie, E.-Y., Edgerton, E., Shaw, S. and Trainer, M.: A volatility basis set model  
763 for summertime secondary organic aerosols over the eastern United States in 2006, *J.*  
764 *Geophys. Res.* 117, D06301, doi:10.1029/2011JD016831, 2012.

765 Beniston, M., Stephenson, D.B., Christensen, O.B., Ferro, C.A.T., Frei, C., Goyette, S.,  
766 Halsnaes, K., Holt, T., Jylha, K., Koffi, B., Palutikof, J., Scholl, R., Semmler, T. and Woth,  
767 K.: Future extreme events in European climate: an exploration of regional climate model  
768 projections, *Clim. Change*, 81, 71 – 95, doi: 10.1007/s10584-006-9226-z, 2007.

769 Bennartz, R.: Global assessment of marine boundary layer cloud droplet number concentration  
770 from satellite, *J. Geophys. Res-Atmos*, 112(D2), D02201, doi:10.1029/2006JD007547, 2007.

771 Brunner, D., Savage, N., Jorba, O., Eder, B., Giordano, L., Badia, A., Balzarini, A., Baro, R.,  
772 Bianconi, R., Chemel, C., Curci, G., Forkel, R., Jimenez-Guerrero, P., Hirtl, M., Hodzic, A.,  
773 Hozak, L., Im, U., Knote, C., Makar, P., Manders-Groot, A., van Meijgaard, E., Neal, L.,  
774 Perez, J.L., Pirovano, G., San Jose, R., Schroder, W., Sokhi, R.S., Syrakov, D., Torian, A.,

775 Tuccella, P., Werhahn, J., Wolke, R., Yahya, K., Zabkar, R., Zhang, Y., Hogrefe, C. and  
776 Galmarini, S.: Comparative analysis of meteorological performance of coupled chemistry-  
777 meteorology models in the context of AQMEII phase 2, *Atmos. Environ.*, in press,  
778 doi:10.1016/j.atmosenv.2014.12.032, 2014.

779 Caldwell, P., H.-N.S. Chin, D.C. Bader, and G. Bala (2009), Evaluation of a WRF dynamical  
780 downscaling simulation over California, *Clim. Change.*, 95, 499-521.

781 Campbell, P. C., Zhang, Y., Yahya, K., Wang, K., Hogrefe, C., Pouliot, G., Knote, C., Hodzic,  
782 A., San Jose, R., Perez, J., Jimenez-Guerrero, P., Baro, R. and Makar, P.: A Multi-Model  
783 Assessment for the 2006 and 2010 Simulations under the Air Quality Model Evaluation  
784 International Initiative (AQMEII) Phase 2 over North America: Part I, Indicators of the  
785 Sensitivity of O<sub>3</sub> and PM<sub>2.5</sub> Formation Regimes, *Atmos. Environ.*, in press,  
786 doi:10.1016/j.atmosenv.2014.12.026, 2014.

787 Chen, F. and Dudhia, J.: Coupling an advanced land-surface/hydrology model with the Penn  
788 State/NCAR MM5 modeling system. Part I: Model implementation and sensitivity. *Mon.*  
789 *Wea. Rev.*, 129, 569-585, 2001.

790 Clough, S.A., Shephard, M.W., Mlawer, J.E., Delamere, J.S., Iacono, M.J., Cady-Pereira, K.,  
791 Boukabara, S. and Brown, P.D.: Atmospheric radiative transfer modeling: a summary of the  
792 AER codes, *J. Quant. Spectrosc. Radiat. Transfer*, 91(2), 233 – 244, doi:  
793 10.1016/j.qsrt.2004.05.058, 2005.

794 Cooper, O.R., Parrish, D.D., Ziemke, J., Balashov, N.V., Cupeiro, M., Galbally, I.E., Gilge, S.,  
795 Horowitz, L., Jensen, N.R., Lamarque, J.-F., Naik, V., Oltmans, S.J., Schwab, J., Shindell,  
796 D.T., Thompson, A.M., Thouret, V., Wang, Y. and Zbinden, R.M.: Global distribution and

797 trends of tropospheric ozone: An observation-based review, *Elem. Sci. Anth.*, 2, 000029,  
798 doi:10.12952/journal.elementa.000029, 2014.

799 Dasari, H.P., Salgado, R., Perdigao, J. and Challa, V.S.: A regional climate simulation study  
800 using WRF-ARW model over Europe and evaluation for extreme temperature weather  
801 events, *Intl. J. of Atmos. Sci.*, ID 704079, doi:10.1155/2014/704079, 2014.

802 Ek, M.B., Mitchell, K.E., Lin, Y., Rogers, E., Grunmann, P., Koren, V., Gayno, G. and Tarpley,  
803 J.D.: Implementation of NOAA land surface model advances in the National Centers for  
804 Environmental Prediction operational mesoscale model, *J. Geophys. Res.*, 108, D22, 8851,  
805 doi:10.1029/2002JD003296, 2003.

806 EPA.: Our Nation's Air – Status and Trends through 2010, Particle Pollution, Report by the U.S.  
807 EPA, 4pp, <http://www.epa.gov/airtrends/2011>, 2011, last accessed July 6<sup>th</sup>, 2015.

808 Fan, F., Bradley, R.S. and Rawlins, M.A.: Climate change in the northeastern U.S.: regional  
809 climate validation and climate change projections, *Clim. Dyn.*, 43, 145 – 161,  
810 doi:10.1007/s00382-014-2198-1, 2014.

811 Feser, F., Rockel, B., Von Storch, H., Winterfeldt, J. and Zahn, M.: Regional climate models add  
812 value to global model data, *Bull. Amer. Meteor. Soc.*, 92, 1181 – 1192, 2011.

813 Flato et al.: Evaluation of Climate Models, In: *Climate Change 2013: The Physical Science*  
814 *Basis. Contribution of Working Group I to the Fifth Assessment Report of the*  
815 *Intergovernmental Panel on Climate Change* [Stocker, T.F., D. Qin, G.-K. Plattner, M.  
816 Tignor, S.K. Allen, J. Boschung, A. Nauels, Y. Xia, V. Bex and P.M. Midgley (eds.)],  
817 Cambridge University Press, Cambridge, United Kingdom and New York, NY, U.S.A.,  
818 2013.

819 Gao, Y., Fu, J.S., Drake, J.B., Liu, Y. and Lamarque, J.F.: Projected changes of extreme weather  
820 events in the eastern United States based on a high resolution climate modeling system,  
821 Environ. Res. Lett., 7, 044025, 2012.

822 Gao, Y., Fu, J.S., Drake, J.B., Lamarque, J.-F. and Liu, Y.: The impact of emission and climate  
823 change on ozone in the United States under representative concentration pathways (RCPs),  
824 Atmos. Chem. Phys., 2013, 9607 – 9621, 2013.

825 Glotfelty, T., He, J. and Zhang, Y.: Updated organic aerosol treatments in CESM/CAM5:  
826 development and initial application, in preparation, 2015.

827 Gong, S., Barrie, L.A. and Blanchet, J.P.: Modeling sea salt aerosols in the atmosphere: 1. Model  
828 development, J. Geophys. Res., 102, 3805-3818, doi:10.1029/96JD02953, 1997.

829 Grell, G.A., Knoche, R., Peckham, S.E. and McKeen, S.A.: Online versus offline air quality  
830 modeling on cloud-resolving time scales, Geophys. Res. Lett., 31 (16),  
831 doi:10.1029/2004GL020175, 2004.

832 Grell, G.A., Peckham, S.E., Schmitz, R., McKeen, S.A., Frost, G., Skamarock, W.C. and Eder,  
833 B.: Fully coupled “online” chemistry within the WRF model, Atmos. Environ., 39, 6957-  
834 6975, 2005.

835 Grell, G.A. and Freitas, S.R.: A scale and aerosol aware stochastic convective parameterization  
836 for weather and air quality modeling, Atmos. Chem. Phys., 14, 5233-5250, doi:10.5914/acp-  
837 14-5233-2014, 2014.

838 Guenther, A., Kart, T., Harley, P., Wiedinmyer, C., Palmer, P.I. and Geron, C.: Estimates of  
839 global terrestrial isoprene emissions using MEGAN (Model of Emissions of Gases and  
840 Aerosols from Nature), Atmos. Chem. Phys., 6, 3181-3210, 2006.

841 He, J., Zhang, Y., Glotfelty, T., He, R., Bennartz, R., Rausch, J. and Sartelet, K.: Decadal  
842 simulation and comprehensive evaluation of CESM/CAM5.1 with advanced chemistry,  
843 aerosol microphysics and aerosol-cloud interactions, *J. Adv. Model. Earth Syst.*, 7, 110 –  
844 141, doi:10.1002/2014MS000360, 2015.

845 Hong, S.-Y., Noh, Y. and Dudhia, J.: A new vertical diffusion package with an explicit treatment  
846 of entrainment processes, *Mon. Wea. Rev.*, 134, 2318-2341, 2006.

847 Hong, S.-Y.: A new stable boundary-layer mixing scheme and its impact on the simulated East  
848 Asian summer monsoon, *Q.J.R. Meteorol. Soc.*, 136, 1481 – 1496, doi:0.1002/qj.665, 2010.

849 Hurrell, J.W., Holland, M.M., Gent, P.R., Ghan, S., Kay, J.E., Kushner, P.J., Lamarque, J.-F.,  
850 Large, W.G., Lawrence, D., Lindsay, K., Lipscomb, W.H., Long, M.C., Mahowald, N.,  
851 Marsh, D.R., Neale, R.B., Rasch, P., Vavrus, S., Vertenstein, M., Bader, D., Collins, W.D.,  
852 Hack, J.J., Kiehl, J. and Marshall, S.: The Community Earth System Model: A framework for  
853 collaborative research, *Bull. Am. Meteorol. Soc.*, 94, 1339 – 1360, doi:10.1175/BAMS-D-  
854 12-00121.1, 2013.

855 Iacono, M.J., Delamere, J.S., Mlawer, E.J., Shepard, M.W., Clough, S.A. and Collins, W.D.:  
856 Radiative forcing by long-lived greenhouse gases: Calculations with the AER radiative  
857 transfer models, *J. Geophys. Res.*, 113, D13103, doi:10.1029/2008JD009944, 2008.

858 IPCC : Climate change 2013: the physical science basis. In: Stocker, T.F., Qin, D., Plattner, G.-  
859 K., Tignor, M.M.B., Allen, S.K., Boschung, J., Nauels, A., Xia, Y., Bex, V., Midgley, P.M.  
860 (Eds.), *Contribution of Working Group I to the Fifth Assessment Report of the*  
861 *Intergovernmental Panel on Climate Change, Summary for Policymakers*, 2013.

862 Jacob, D., Barring, L., Christensen, O.B., Christensen, J.H., de Castro, M., Deque, M., Giorgi, F.,  
863 Hagemann, S., Hirschi, M., Jones, R., Kjellstrom, E., Lenderink, G., Rockel, B., Sanchez, E.,

864 Schar, C., Seneviratne, S.I., Somot, S., van Ulden, A. and van den Hurk, B.: An inter-  
865 comparison of regional climate models for Europe: model performance in present-day  
866 climate, *Clim. Change*, 81, 31 – 52, 2007.

867 Jimenez, P.A. and Dudhia, J.: Improving the representation of resolved and unresolved  
868 topographic effects on surface wind in the WRF model, *J. Appl. Meteor. Climatol.*, 51, 300 –  
869 316, 2012.

870 Jones, R.G., Noguer, M., Hassell, D.C., Hudson, D., Wilson, S.S., Jenkins G.J. and Mitchell,  
871 J.F.B.: Generating high resolution climate change scenarios using PRECIS, Met Office  
872 Hadley Centre, Exeter, UK, 40 pp., April 2004, 2004.

873 Jones, S. and Creighton, G.: AFWA dust emission scheme for WRF/Chem-GOCART, 2011  
874 WRF workshop, June 20-24, Boulder, CO, USA, 2011.

875 Karamchandani, P., Zhang, Y., Chen, S.-Y., and Balmori-Bronson, R.: Development of an  
876 extended chemical mechanism for global-through-urban applications, *Atmos. Poll. Res.*, 3, 1  
877 – 24, doi:10.5094/apr.2011.047.

878 Kim, J., Waliser, D.E., Mattmann, C.A., Mearns, L.O., Goodale, C.E., Hart, A.F., Crichton,  
879 D.J., McGinnis, S., Lee, H., Loikith, P.C. and Boustani, M.: Evaluation of the surface  
880 climatology over the conterminous United States in the North American Regional Climate  
881 Change Assessment Program Hindcast Experiment using a regional climate model evaluation  
882 system, *J. Climate*, 26, 5698 – 5715, 2013.

883 King, N.J., Bower, K.N., Crosier, J. and Crawford, I.: Evaluating MODIS cloud retrievals with in  
884 situ observations from VOCALS-REx, *Atmos. Chem. Phys.*, 13, 191 – 209, 2013.

885 Legates, D.R. and McCabe Jr., G.J.: Evaluating the use of “goodness-of-fit” measures in  
886 hydrologic and hydroclimatic model validation, *Water Resour. Res.*, 35(1), 233 – 241,  
887 doi:10.1029/1998WR900018, 1999.

888 Levy, R.C., Remer, L.A. and Dubovik, O.: Global aerosol optical properties and application to  
889 Moderate Resolution Imaging Spectroradiometer aerosol retrieval over land, *J. Geophys.*  
890 *Res.*, 112(D13), doi:10.1029/2006JD007815, 2007.

891 Levy, R.C., Mattoo, S., Muchak, L.A., Remer, L.A., Sayer, A.M., Patadia, F., Hsu, N.C.: The  
892 Collection 6 MODIS aerosol products over land and ocean, *Atmos. Meas. Tech.*, 6, 2989 –  
893 3034, 2013.

894 Leung, R.L., Qian, Y. and Bian, X.: Hydroclimate of the Western United States based on  
895 Observations and Regional Climate Simulation of 1981 – 2000, Part I: Seasonal Statistics, *J.*  
896 *Clim.*, 16(12), 1892 – 1911, 2003.

897 Liu, X., Easter, R.C., Ghan, S.J., Zaveri, R., Rasch, P., Shi, X., Lamarque, J.-F., Gettelman, A.,  
898 Morrison, H., Vitt, F., Conley, A., Park, S., Neale, R., Hannay, C., Ekman, A.M.L., Hess, P.,  
899 Mahowald, N., Collins, W., Iacono, M.J., Bretherton, C.S., Flanner, M.G., and Mitchell, D.:  
900 Toward a minimal representation of aerosols in climate models: description and evaluation in  
901 the Community Atmosphere Model CAM5, *Geosci. Mod. Dev.*, 5, 709 – 739,  
902 doi:10.5194/gmd-5-709-2012, 2012.

903 Loeb, N.G., Wielicki, B.A., Doelling, D.R., Smith, L., Keyes, D.F., Kato, S., Manalo-Smith, N.  
904 and Wong, T.: Toward Optimal Closure of the earth’s top-of-atmosphere radiation budget, *J.*  
905 *Climate*, 22, 748 – 766, 2009.

906 Ma, P.-L., Rasch, P.J., Fast, J.D., Easter, R.C., Gustafson Jr., W.I., Liu, X., Ghan, S.J. and Singh,  
907 B.: Assessing the CAM5 physics suite in the WRF-Chem model: implementation, resolution

908 sensitivity, and a first evaluation for a regional case study, *Geosci. Model Dec.*, 7, 755 – 778,  
909 2014.

910 Mass, C.: Improved subgrid drag or hyper PBL/vertical resolution? Dealing with the stable PBL  
911 problems in WRF, presented at the 13<sup>th</sup> WRF Users' Workshop, June 26 – 29, Boulder, CO,  
912 2012.

913 Molders, N., Bruyere, C.L., Gende, S. and Pirhala, M.A.: Assessment of the 2006-2012  
914 Climatological Fields and Mesoscale Features from Regional Downscaling of CESM Data by  
915 WRF/Chem over Southeast Alaska, *Atmos. Clim. Sci.*, 4, 589 – 613, 2014.

916 Morrison, H., Thompson, G. and Tatarskii, V.: Impact of cloud microphysics on the development  
917 of trailing stratiform precipitation in a simulated squall line: Comparison of One- and Two-  
918 Moment Schemes, *Mon. Wea. Rev.*, 137, 991-1007, 2009.

919 Moss, R. H., Edmonds, J.A., Hibbard, K.A., Manning, M.R., Rose, S.K., van Vuuren, D.P.,  
920 Carter, T.R., Emori, S., Kainuma, M., Kram, T., Meehl, G.A., Mitchell, J.F.B., Nakicenovic,  
921 N., Riahi, K., Smith, S.J., Stouffer, R.J., Thomson, A.M., Weyant, J.P. and Wilbanks, T.J.:  
922 The next generation of scenarios for climate change research and assessment, *Nature*, 463,  
923 747 – 756, doi: 10.1038/nature0882, 2010.

924 Nasrollahi, N., AghaKouchak, A., Li, J., Gao, X., Hsu, K. and Sorooshian, S.: Assessing the  
925 Impacts of Different WRF Precipitation Physics in Hurricane Simulations, *Wea. Forecasting*,  
926 27, 1003 – 1016, 2012.

927 Neale R.B., Jadwiga, H.R., Conley, A.J., Park, S., Lauritzen, P.H., Gettelman, A., Williamson,  
928 D.L., Rasch, P., Vavrus, S.J., Taylor, M.A., Collins, W.D., Zhang, M. and Lin, S.-J.:  
929 Description of the NCAR Community Atmosphere Model (CAM 5.0), NCAR Tech. Note  
930 NCAR/TN-486+STR, Natl. Cent. for. Atmos. Res., Boulder, CO, available at

931 [http://www.cesm.ucar.edu/models/cesm1.0/cam/docs/description/cam5\\_desc.pdf](http://www.cesm.ucar.edu/models/cesm1.0/cam/docs/description/cam5_desc.pdf), 2010, last  
932 accessed July 6<sup>th</sup>, 2015.

933 Otte, T.L., Nolte, C.G., Otte, M.J. and Bowden, J.H.: Does Nudging squelch the extremes in  
934 regional climate modeling? *J. Clim.*, 25, 7046 – 7066, doi:10.1175/JCLI-D-12-00048.1,  
935 2012.

936 Penrod, A., Zhang, Y., Wang, K., Wu, S-Y. and Leung, R.L.: Impacts of future climate and  
937 emission changes on U.S. air quality, *Atmos. Environ.*, 89, 533 – 547, 2014.

938 Petikainen, J.-P., O'Donnell, D., Teichmann, C., Karstens, U., Pfeifer, S., Kazil, J., Podzun, R.,  
939 Fiedler, S., Kokkola, H., Birmili, W., O'Dowd, C., Baltensperger, U., Weingartner, E.,  
940 Gehrig, R., Spindler, G., Kulmala, M., Feichter, J., Jacob, D. and Laaksonen, A.: The  
941 regional aerosol-climate model REMO-HAM, *Geosci. Mod. Dev.*, 5, 1323 – 1339, 2012.

942 Pleim, J.E. and Gilliam, R.: An indirect data assimilation scheme for deep soil temperature in the  
943 Pleim-Xiu Land Surface Model, *J. Appl. Meteor. Climatol.*, 48, 1362 – 1376, 2009.

944 Pouliot, G., van der Gon, H.A.C.D., Kuenen, J., Zhang, J., Moran, M. and Makar, P.: Analysis of  
945 the Emission Inventories and Model-Ready Emission Datasets of Europe and North America  
946 for Phase 2 of the AQMEII Project, *Atmos. Environ.*, in press,  
947 doi:10.1016/j.atmosenv.2014.10.061, 2014.

948 Rawlins, M.A., Bradley, R.S. and Diaz, H.F.: Assessment of regional climate model simulation  
949 estimates over the northeast United States, *J. Geophys. Res.*, 117, D23112,  
950 doi:10.1029/2012JD018137, 2012.

951 Refslund, J., Dellwik, E., Hahmann, A.N., Barlage, M.J. and Boegh, E.: Development of satellite  
952 green vegetation fraction time series for use in mesoscale modeling: application to the

953 European heat wave 2006, *Theor. Appl. Climatol.*, 117, 377-392, doi:10.1007/s00704-013-  
954 1004-z, 2014.

955 Sarwar, G., Luecken, D.J. and Yarwood, G.: Developing and implementing an updated chlorine  
956 chemistry into the Community Multiscale Air Quality Model, presented at the 28<sup>th</sup>  
957 NATO/CCMS International Technical Meeting, Leipzig, Germany, May 15 – 19, 2006.

958 Sarwar, G., Luecken, D. and Yarwood, G.: Chapter 2.9: Developing and implementing an  
959 updated chlorine chemistry into the community multiscale air quality model, *Developments*  
960 *in Environmental Science*, Volume 6, C. Borrego and E. Renner (Eds.), Elsevier Ltd,  
961 DOI:10.1016/S1474-8177(07)06029-9, 168 pp., 2007.

962 Sarwar, G., Fahey, K., Napelenok, S., Roselle, S. and Mathur, R.: Examining the impact of  
963 CMAQ model updates on aerosol sulfate predictions, the 10<sup>th</sup> Annual CMAS Models-3  
964 User's Conference, October, Chapel Hill, NC, 2011.

965 Shan, Z., Parol, F., Riedi, J., Cornet, C. and Thieuleux, F.: Examination of POLDER/PARASOL  
966 and MODIS/Aqua cloud fractions and properties representativeness, *J. Climate*, 24, 4435 –  
967 4450, 2011.

968 Sievering, H.: Small-particle dry deposition under high wind speed conditions: Eddy flux  
969 measurements at the boulder atmospheric observatory, *Atmos. Environ.*, 21 (10), 2179 –  
970 2185, 1987.

971 Tewari, M., Chen, F., Wang, W., Dudhia, J., LeMone, M.A., Mitchell, K., Ek, M., Gayno, G.,  
972 Wegiel, J. and Cuenca, R.H.: Implementation and verification of the unified NOAA land  
973 surface model in the WRF model. 20<sup>th</sup> conference on weather analysis and forecasting/16<sup>th</sup>  
974 conference on numerical weather prediction, pp. 11 – 15, 2004.

975 Toth, T.D., Zhang, J., Campbell, J.R., Reid, J.S., Shi, Y., Johnson, R.S., Smirnov, A., Vaughan,  
976 M.A. and Winker, D.M.: Investigating enhanced Aqua MODIS aerosol optical depth  
977 retrievals over the mid-to-high latitude Southern Oceans through intercomparison with co-  
978 located CALIOP, MAN and AERONET data sets, *J. Geophys. Res: Atmos*, 18, 1- 15, 2013.

979 van Vuuren, D.P., Edmonds, J., Kainuma, M., Riahi, K., Thomson, A., Hibbard, K., Hurtt, G.C.,  
980 Kram, T., Krey, V., Lamarque, J.-F., Masui, T., Meinshausen, M., Nakicenovic, N., Smith,  
981 S.J. and Rose, S.K.: The representative concentration pathways: an overview, *Climate*  
982 *Change*, 109, 5 – 31, doi: 10.1007/s10584-011-0148-z, 2011.

983 Wang, K., Zhang, Y., Yahya, K., Wu, S.-Y. and Grell, G.: Implementation and initial  
984 application of new chemistry-aerosol options in WRF/Chem for simulating secondary  
985 organic aerosols and aerosol indirect effects for regional air quality, *Atmos. Environ.*, in  
986 press, doi: 10.1016/j.atmosenv.2014.12.007, 2014a.

987 Wang, K., Yahya, K., Zhang, Y., Hogrefe, C., Pouliot, G., Knote, C., Hodzic, A., San Jose, R.,  
988 Perez, J.L., Guerrero, P.J., Baro, R. and Makar, P.: Evaluation of Column Variable  
989 Predictions Using Satellite Data over the Continental United States: A Multi-Model  
990 Assessment for the 2006 and 2010 Simulations under the Air Quality Model Evaluation  
991 International Initiative (AQMEII) Phase 2, *Atmos. Environ.*, in press,  
992 doi:10.1016/j.atmosenv.2014.07.044, 2014b.

993 Warrach-Sagi, K., Schwitalla, T., Wulfmeyer, V. and Bauer, H.-S.: Evaluation of a climate  
994 simulation in Europe based on the WRF-NOAH model system: precipitation in Germany,  
995 *Clim. Dyn.*, 41, 755 – 774, doi:10.1007/s00382-013-1727-7, 2013.

996 Willmott, C. J.: On the validation of models, *Phys. Geog.*, 2, 184 – 194, 1981.

997 Xing, J., Mathur, R., Pleim, J., Hogrefe, C., Gan, C.-M., Wong, D.C., Wei, C., Gilliam, R. and  
998 Pouliot, G.: Observations and modeling of air quality trends over 1990-2010 across the  
999 Northern Hemisphere: China, the United States and Europe, *Atmos. Chem. Phys.*, 15, 2723 –  
1000 2747, doi:10.5194/acp-15-2723-2015.

1001 Xu, Z. and Yang, Z.-L.: An improved dynamical downscaling method with GCM Bias  
1002 Corrections and Its Validation with 30 years of climate simulations, *J. Clim.*, 25, 6271 –  
1003 6286, 2012.

1004 Yahya, K., Wang, K., Gudoshava, M., Glotfelty, T. and Zhang, Y.: Application of WRF/Chem  
1005 over North America under the AQMEII Phase 2. Part I. Comprehensive Evaluation of 2006  
1006 Simulation, *Atmospheric Environment*, in press, doi:10.1016/j.atmosenv.2014.08.063, 2014.

1007 Yahya, K., He, J., and Zhang, Y.: Multi-Year Applications of WRF/Chem over Continental U.S.:  
1008 Model Evaluation, Variation Trend, and Impacts of Boundary Conditions over CONUS, *J.*  
1009 *Geophys. Res.*, in review, 2015a.

1010 Yahya, K., Wang, K., Zhang, Y. and Kleindienst, T.E.: Application of WRF/Chem over North  
1011 America under the AQMEII Phase 2. Part II. Comprehensive Evaluation of 2010 Simulation  
1012 and Responses of Air Quality and Meteorology-Chemistry Interactions to Changes in  
1013 Emissions and Meteorology from 2006 to 2010, *Geosci. Model Dev.*, in press, 2015b.

1014 Yarwood, G., Rao, S., Yocke, M. and Whitten, G.Z.: Final Report – Updates to the Carbon Bond  
1015 Chemical Mechanism: CB05, Rep. RT-04-00675, 246 pp., Yocke and Co., Novato, Calif.,  
1016 2005.

1017 Yu, S., Dennis, R., Roselle, S., Nenes, A., Walker, J., Eder, B., Schere, K., Swall, J., and  
1018 Robarge, W.: An assessment of the ability of 3-D air quality models with current

1019 thermodynamic equilibrium models to predict aerosol NO<sub>3</sub><sup>-</sup>, *J. Geophys. Res.*, 110, D07S13,  
1020 doi:10.1029/2004JD004718, 2005.

1021 Yu, S., Eder, B., Dennis, R., Chu, S.-H., and Schwartz, S.: New unbiased symmetric metrics for  
1022 evaluation of air quality models, *Atmos. Sci. Lett.*, 7, 26 – 34, 2006.

1023 Yu, S., Mathur, R., Pleim, J., Wong, D., Gilliam, R., Alapaty, K., Zhao, C., and Liu, X.: Aerosol  
1024 indirect effect on the grid-scale clouds in the two-way coupled WRF-CMAQ: model  
1025 description, development, evaluation and regional analysis, *Atmos. Chem. Phys.*, 14, 11247 –  
1026 11285, doi:10.5194/acp-14-1-2014, 2014.

1027 Zhang, Y., Liu, P., Pun, B., and Seigneur, C.: A comprehensive performance evaluation of  
1028 MM5-CMAQ for summer 1999 Southern Oxidants Study Episode, Part-I. Evaluation  
1029 Protocols, Databases and Meteorological Predictions, *Atmos. Environ.*, 40, 4825 – 4838,  
1030 2006.

1031 Zhang, Y., Wen, X.-Y. and Jang, C.J.: Simulating chemistry-aerosol-cloud-radiation-climate  
1032 feedbacks over the CONUS using the online-coupled Weather Research Forecasting Model  
1033 with chemistry (WRF/Chem), *Atmos. Environ.*, 44, 3568 – 3582, 2010.

1034 Zhang, Y., Y.-C. Chen, G. Sarwar, and K. Schere, 2012a, Impact of Gas-Phase Mechanisms on  
1035 Weather Research Forecasting Model with Chemistry (WRF/Chem) Predictions: Mechanism  
1036 Implementation and Comparative Evaluation, *J. Geophys. Res.*, 117, D1,  
1037 doi:10.1029/2011JD015775.

1038 Zhang, Y., P. Karamchandani, T. Glotfelty, D. G. Streets, G. Grell, A. Nenes, F.-Q. Yu, and R.  
1039 Bennartz, 2012b, Development and Initial Application of the Global-Through-Urban  
1040 Weather Research and Forecasting Model with Chemistry (GU-WRF/Chem), *J. Geophys.*  
1041 *Res.*, 117, D20206, doi:10.1029/2012JD017966.

Table 1. Model configurations and set-up

<b>Model Attribute</b>	<b>Configuration</b>	<b>Reference</b>
<b>Domain and Resolutions</b>	36km × 36km, 148 × 112 horizontal resolution over continental U.S., with 34 layers vertically from surface to 100 hPa	-
<b>Simulation Period</b>	January 2001 to December 2010	-
<b>Chemical and Meteorological ICs/BCs</b>	Downscaled from the modified Community Earth System Model/Community Atmosphere Model (CESM/CAM5) v1.2.2; Meteorological ICs/BCs bias-corrected with National Center for Environmental Protection's Final (FNL) Operational Global Analysis data	He et al. (2014) Glotfelty et al. (2015)
<b>Biogenic Emissions</b>	Model of Emissions of Gases and Aerosols from Nature (MEGAN2)	Guenther et al. (2006)
<b>Dust Emissions</b>	Atmospheric and Environmental Research Inc. and Air Force Weather Agency (AER/AFWA)	Jones and Creighton (2011)
<b>Sea-Salt Emissions</b>	Gong et al. parameterization	Gong et al. (1997)
<b>Radiation</b>	Rapid and accurate Radiative Transfer Model for GCM (RRTMG) SW and LW	Clough et al. (2005) Iacono et al. (2008)
<b>Boundary Layer</b>	Yonsei University (YSU)	Hong et al. (2006) Hong (2010)
<b>Land Surface</b>	National Center for Environmental Prediction, Oregon State University, Air Force and Hydrologic Research Lab (NOAH)	Chen and Dudhia (2001) Ek et al. (2003) Tewari et al. (2004)
<b>Microphysics</b>	Morrison double moment scheme	Morrison et al. (2009)
<b>Cumulus Parameterization</b>	Grell 3D Ensemble	Grell and Freitas (2014)
<b>Gas-phase chemistry</b>	Modified CB05 with updated chlorine chemistry	Yarwood et al. (2005) Sarwar et al. (2006) Sarwar et al. (2007)
<b>Photolysis</b>	Fast Troposphere Ultraviolet Visible (FTUV)	Tie et al. (2003)
<b>Aqueous-phase chemistry</b>	AQ chemistry module (AQCHEM) for both resolved and convective clouds	Based on AQCHEM in CMAQv4.7 of (Sarwar et al. 2011)
<b>Aerosol module</b>	MADE/VBS	Ahmadov et al. (2012)
<b>Aerosol Activation</b>	Abdul-Razzak and Ghan	Abdul-Razzak and Ghan (2000)

Table 2. The 10-year (2001 – 2010) average performance statistics for the simulated meteorological, aerosol, cloud, radiation variables, and chemical species against surface observational networks and satellite retrieval products.

Database and Variable	Mean Obs	Mean Sim	R	MB	NMB (%)	NME (%)
NCDC T2 (°C)	12.5	12.2	1.0	-0.3	-2.6	7.9
NCDC RH2 (%)	68.4	70.8	0.8	2.4	3.5	6.8
NCDC WS10 (m s <sup>-1</sup> )	3.54	3.84	0.3	0.3	8.6	28.4
NCDC WD10 (deg)	151.4	180.0	0.2	28.6	18.9	22.0
NADP Precip (mm day <sup>-1</sup> )	18.0	26.3	0.5	8.3	45.9	65.1
CERES SWDOWN (W m <sup>-2</sup> )	184.1	184.6	0.8	0.5	0.3	8.4
CERES GSW (W m <sup>-2</sup> )	157.5	151.8	0.8	-5.7	-3.6	9.6
CERES GLW (W m <sup>-2</sup> )	323.3	325.7	1.0	2.4	0.7	1.8
CERES OLR (W m <sup>-2</sup> )	240.0	224.8	0.6	-15.0	-6.3	6.3
MODIS AOD	0.14	0.10	0.1	-0.03	-24.0	38.5
MODIS CLDFRA	58.3	62.0	0.7	3.7	6.4	11.9
MODIS-derived CDNC (cm <sup>-3</sup> )	169.8	130.0	0.4	-39.9	-23.5	38.0
MODIS CWP (g m <sup>-2</sup> )	179.5	170.0	0.3	-9.6	-5.3	61.2
MODIS COT	16.5	9.2	0.2	-7.3	-44.3	54.0
CERES SWCF (W m <sup>-2</sup> )	-41.8	-49.6	0.5	7.8	18.6	31.4
CERES LWCF (W m <sup>-2</sup> )	24.8	31.8	0.6	6.9	28.0	34.7
AQS Hourly O <sub>3</sub> (ppb)	29.3	32.1	0.6	2.8	9.7	22.4
AQS Max 1-hr O <sub>3</sub> (ppb)	48.9	49.7	0.6	0.8	1.7	7.9
AQS Max 8-hr O <sub>3</sub> (ppb)	43.7	45.9	0.6	2.2	5.0	9.3
CASTNET Hourly O <sub>3</sub> (ppb)	35.0	31.9	0.7	-3.1	-8.8	19.8
CASTNET Max-1hr O <sub>3</sub> (ppb)	47.4	38.5	0.4	-8.9	-18.8	31.4
CASTNET Max 8-hr O <sub>3</sub> (ppb)	43.3	37.9	0.5	-5.4	-12.5	29.6
AQS 24-hr PM <sub>10</sub> (µg m <sup>-3</sup> )	22.5	11.0	0.1	-11.5	-51.2	57.1
IMPROVE PM <sub>2.5</sub> (µg m <sup>-3</sup> )	5.33	6.57	0.4	1.2	23.3	53.4
STN PM <sub>2.5</sub> (µg m <sup>-3</sup> )	12.0	10.7	0.2	-1.3	-10.8	38.3
IMPROVE SO <sub>4</sub> <sup>2-</sup> (µg m <sup>-3</sup> )	1.45	1.86	0.8	0.4	28.0	41.8
STN SO <sub>4</sub> <sup>2-</sup> (µg m <sup>-3</sup> )	3.10	3.74	0.7	0.6	20.7	36.8
IMPROVE <sup>1</sup> NO <sub>3</sub> <sup>-</sup> (µg m <sup>-3</sup> )	0.54	0.44	0.7	-0.1	-17.9	64.6
STN NO <sub>3</sub> <sup>-</sup> (µg m <sup>-3</sup> )	1.62	0.70	0.4	-0.9	-56.9	65.3
IMPROVE NH <sub>4</sub> <sup>+</sup> (µg m <sup>-3</sup> )	1.02	0.72	0.4	-0.3	-29.6	45.5
STN NH <sub>4</sub> <sup>+</sup> (µg m <sup>-3</sup> )	1.34	1.05	0.5	-0.3	-21.5	38.7
IMPROVE EC (µg m <sup>-3</sup> )	0.23	0.16	0.6	-0.1	-30.7	48.3
STN EC (µg m <sup>-3</sup> )	0.65	0.38	0.2	-0.3	-42.0	52.8
IMPROVE OC (µg m <sup>-3</sup> )	1.10	1.88	0.2	0.8	71.7	134.6
IMPROVE TC (µg m <sup>-3</sup> )	1.33	2.05	0.2	0.7	53.9	116.3
STN TC (µg m <sup>-3</sup> )	4.42	2.42	0.1	-2.0	-45.3	69.7

<sup>1</sup> NH<sub>4</sub><sup>+</sup> IMPROVE data only available up to 2005.

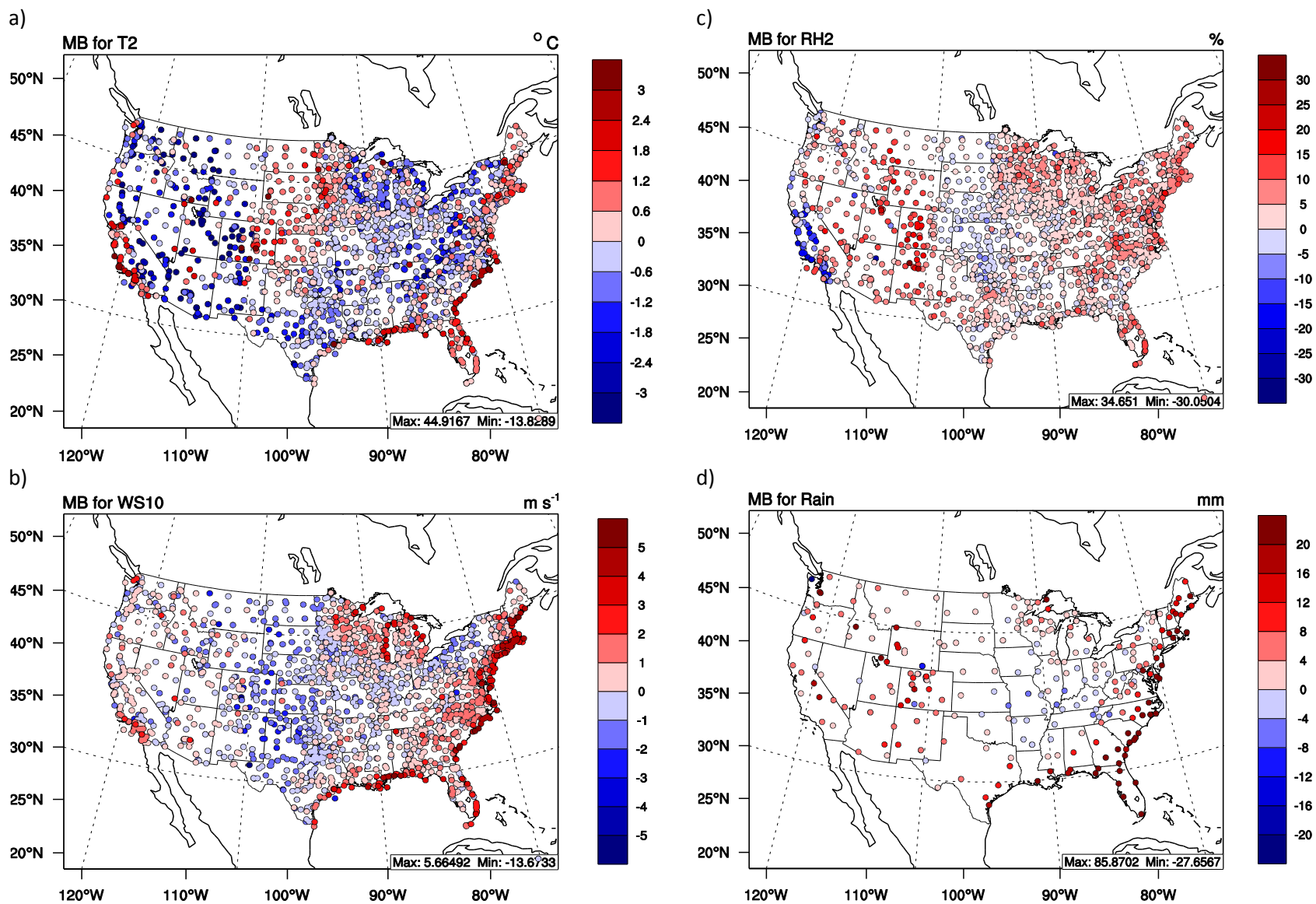


Figure 1. Spatial distribution of MBs for: a) 2-m temperature (T2), b) 2-m relative humidity (RH2), c) 10-m wind speed (WS10) from NCDC, and d) weekly precipitation from NADP. Each marker represents the MB of each variable at each observational site.

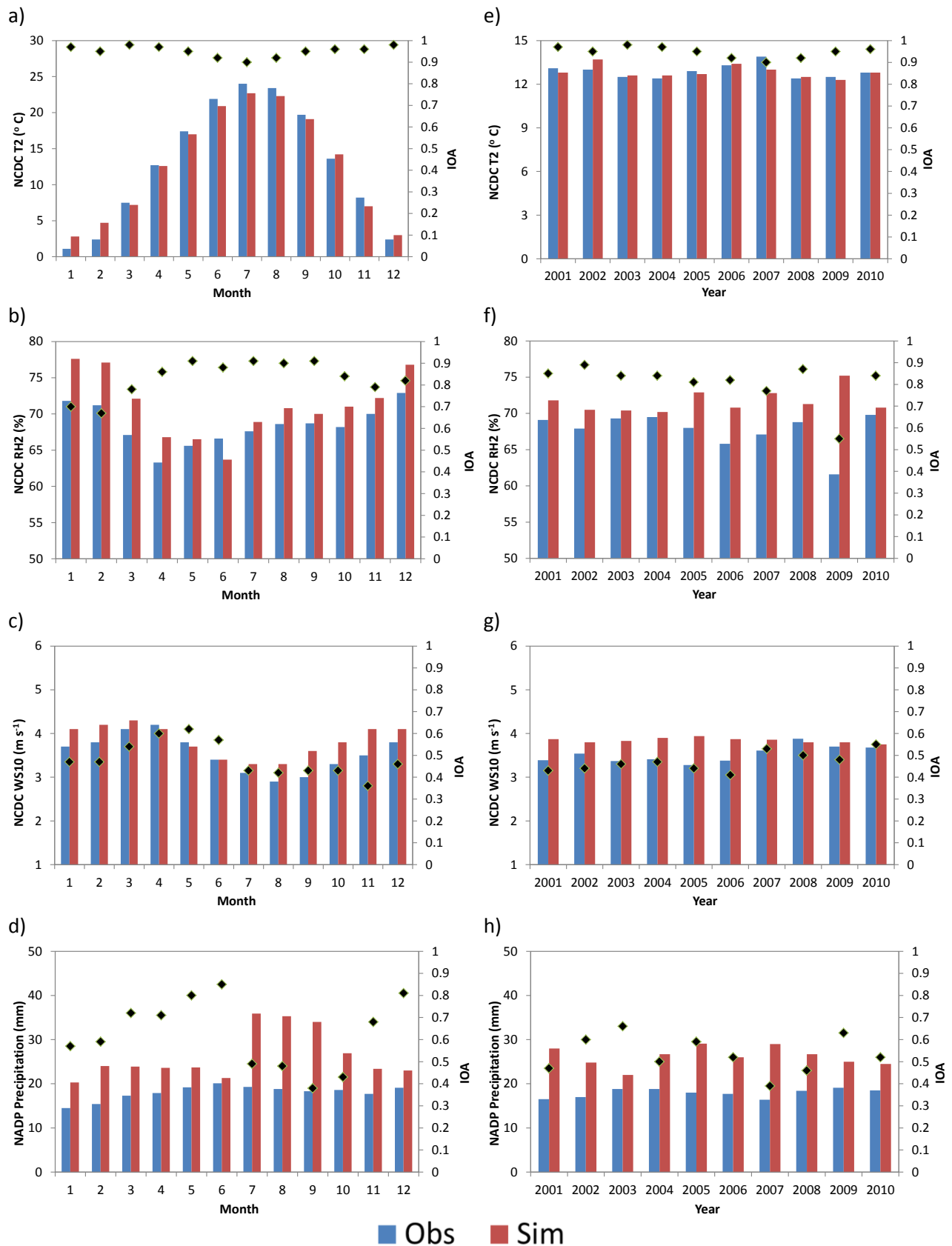


Figure 2. Time series of 10-year averaged monthly observations (blue) versus simulations (red) for: a) T2, b) RH2, and c) WS10 against NCDC data, and d) precipitation against NADP data, and annual averages for e) T2, f) RH2, and g) WS10 against NCDC data, and h) precipitation against NADP. IOA statistics (black diamonds) are also provided on the secondary y-axes in panels a) – h).

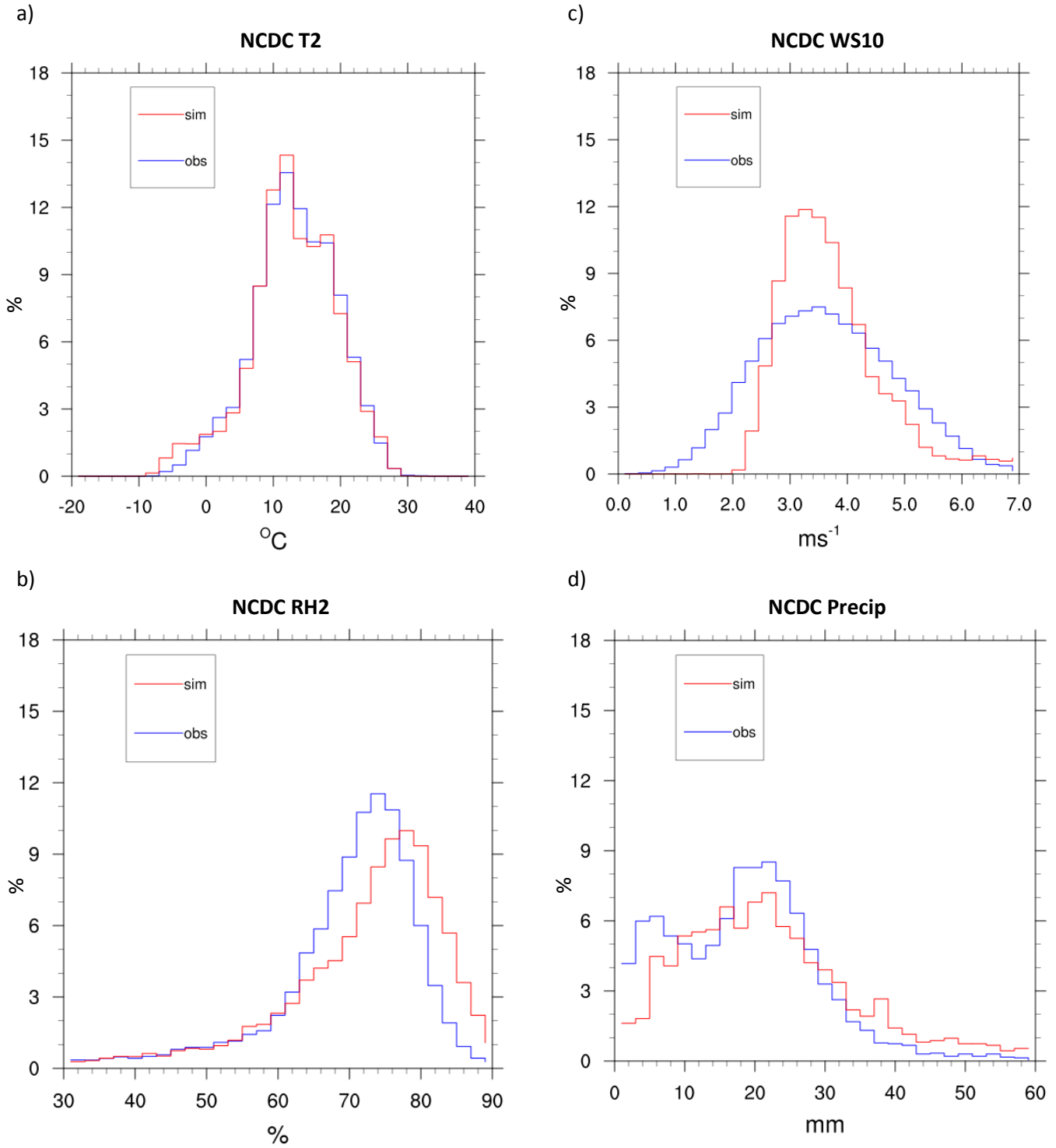


Figure 3. Probability distribution functions (PDFs) of a) T2, b) RH2, c) WS10 against NCDC, and d) precipitation against NADP for 2001 to 2010 over 30 bins in the respective ranges for all variables.

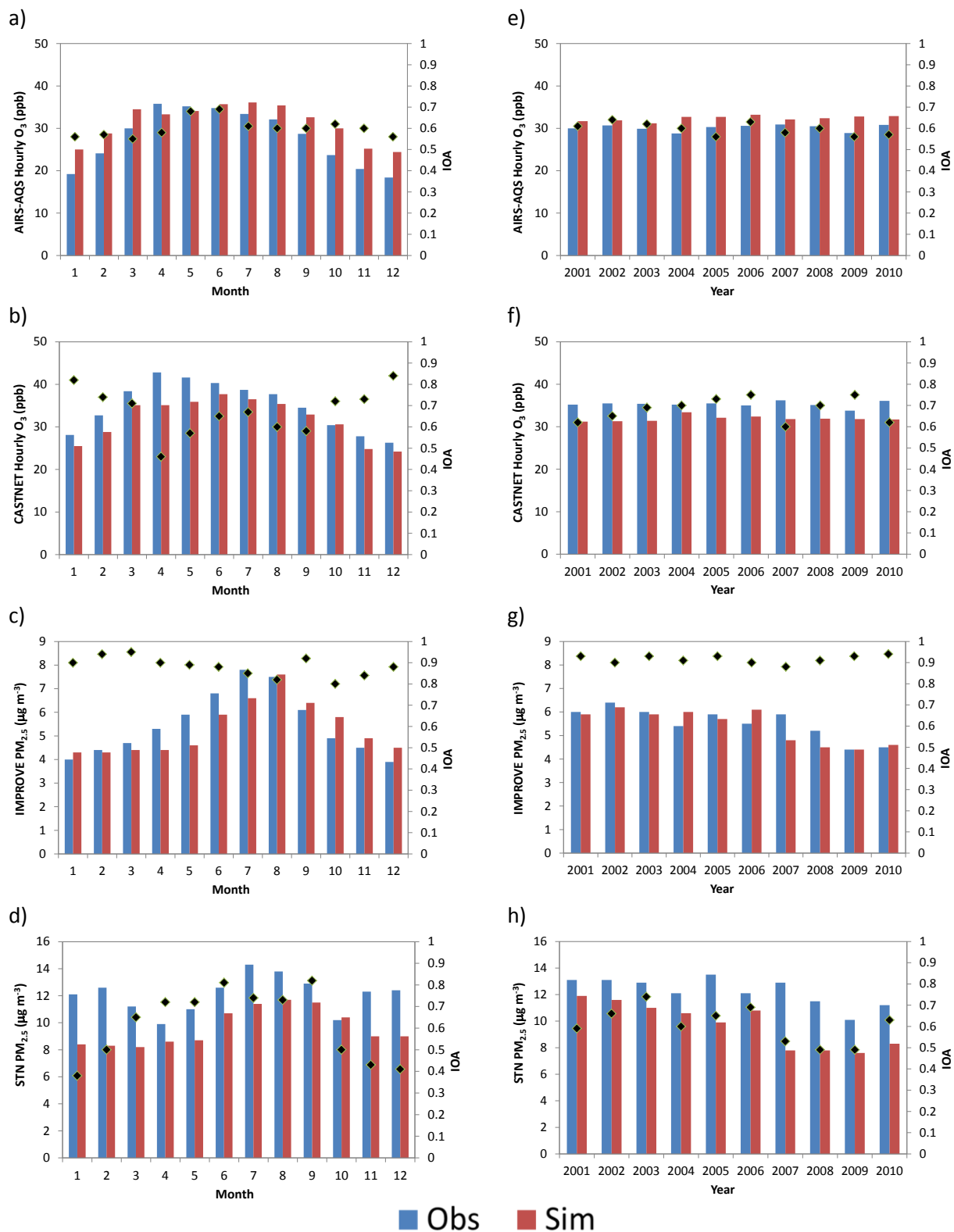


Figure 4. Time series of 10-year averaged monthly-mean observations (blue) versus simulations (red) for: a) O<sub>3</sub> against AQS data, b) O<sub>3</sub> against CASTNET data, c) PM<sub>2.5</sub> against IMPROVE, and d) PM<sub>2.5</sub> against STN, and annual averages for e) O<sub>3</sub> against AQS data, f) O<sub>3</sub> against CASTNET data, g) PM<sub>2.5</sub> against IMPROVE, and h) PM<sub>2.5</sub> against STN. IOA statistics (black diamonds) are also provided on the secondary y-axes in panels a) – h).

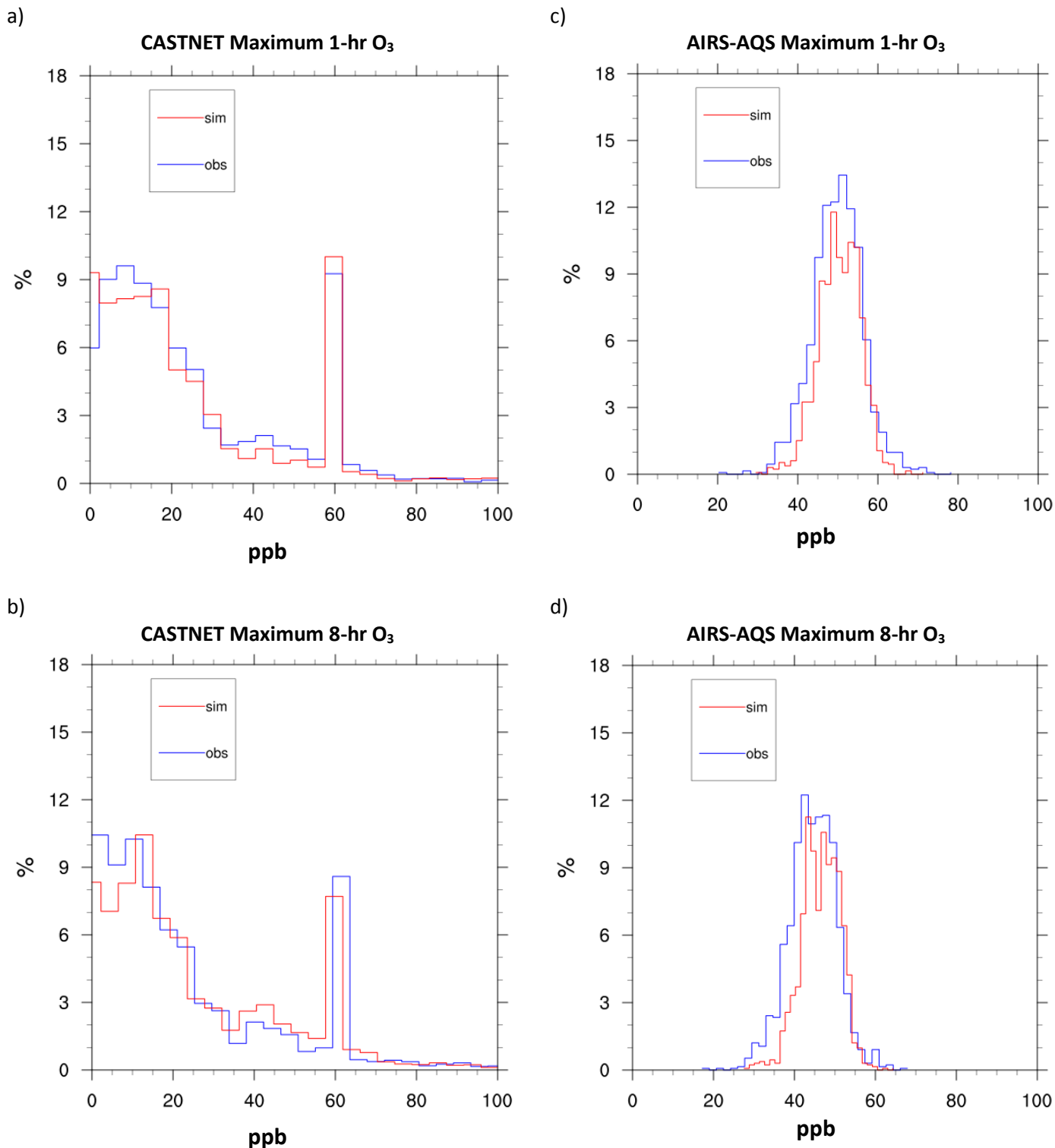


Figure 5. Probability distribution functions (PDFs) of a) maximum 1-hr O<sub>3</sub> against CASTNET, b) maximum 8-hr O<sub>3</sub> against CASTNET, c) maximum 1-hr O<sub>3</sub> against AIRS-AQS, and d) maximum 8-hr O<sub>3</sub> against AIRS-AQS for 2001 to 2010 over 30 bins in the respective ranges for all variables.

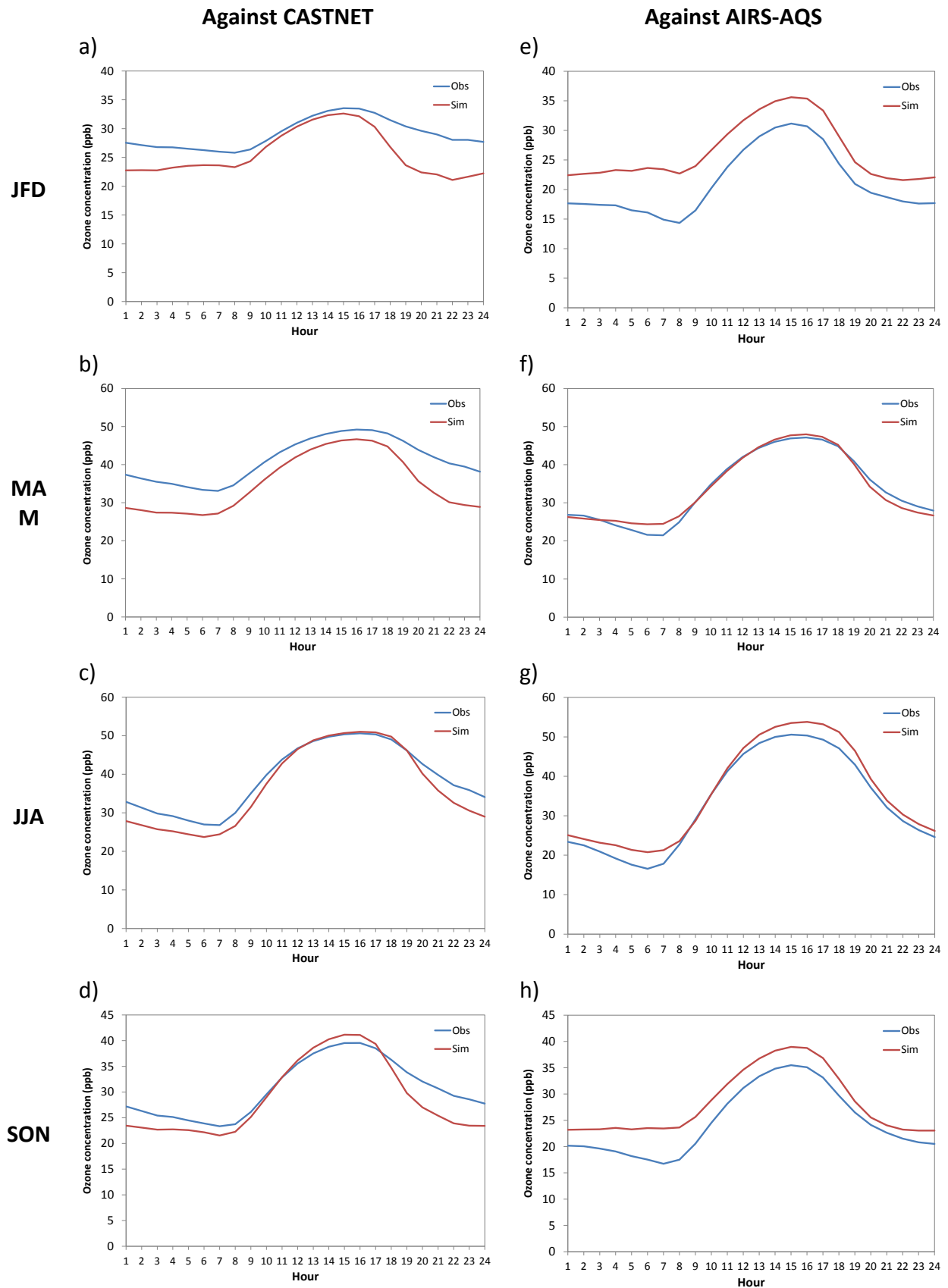


Figure 6. Diurnal variation of observed vs. simulated hourly  $O_3$  concentrations against CASTNET (left column from a) to d)) and AIRS-AQS (right column from e) to h)) for all climatological seasons. The x-axes refer to hours in local standard time.

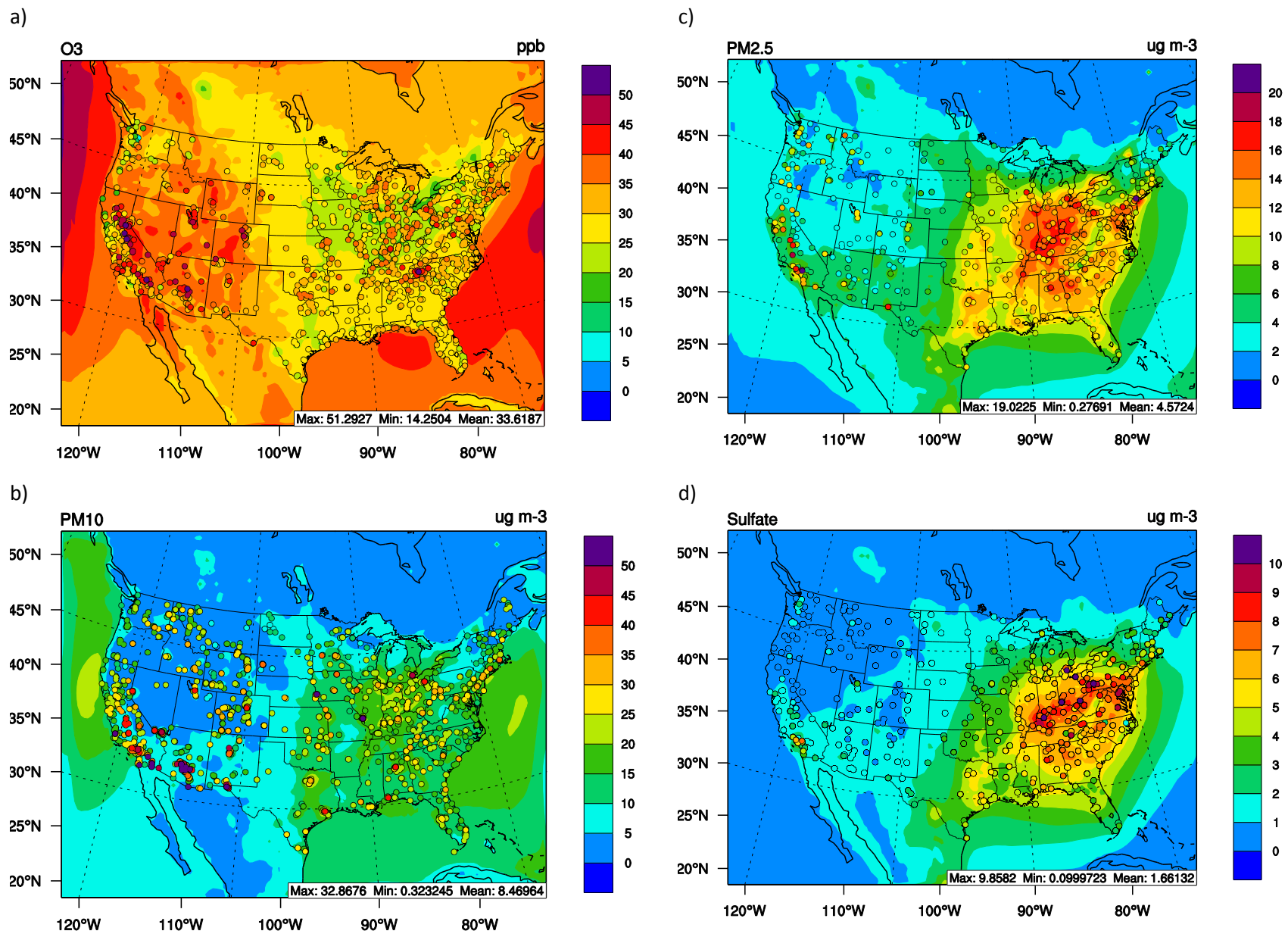


Figure 7. Spatial distribution of 10-year averaged hourly observed vs. simulated a) O<sub>3</sub> for CASTNET and AIRS-AQS, b) PM<sub>10</sub> from AIRS-AQS, c) PM<sub>2.5</sub>, and d) PM<sub>2.5</sub> sulfate from STN and IMPROVE. The background plots represent the simulated data while observations are represented by the markers.

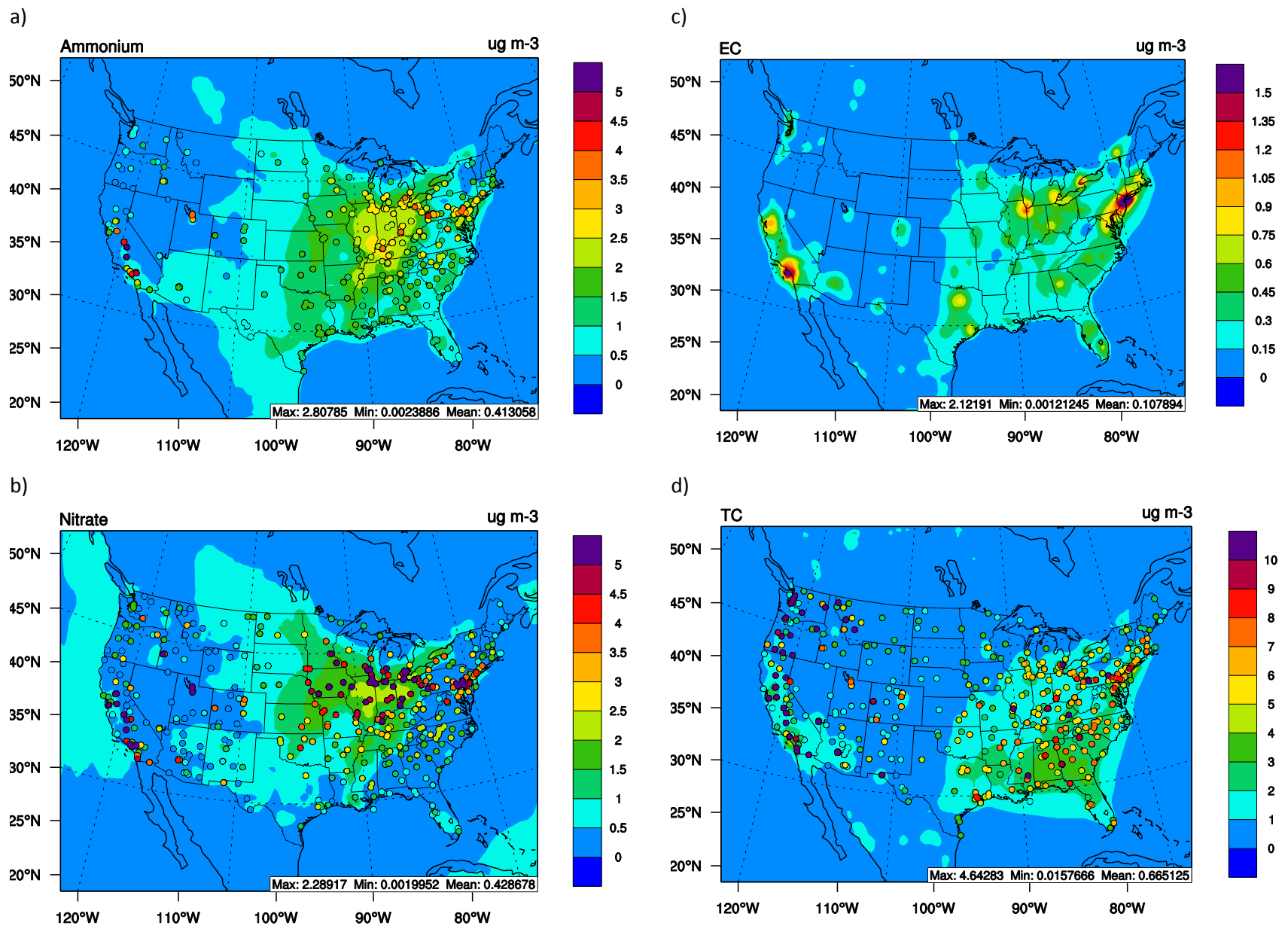


Figure 8. Spatial distribution of 10-year averaged hourly observed vs. simulated a) Ammonium, b) Nitrate, c) EC, and d) TC from STN and IMPROVE. The background plots represent the simulated data while observations are represented by the markers.

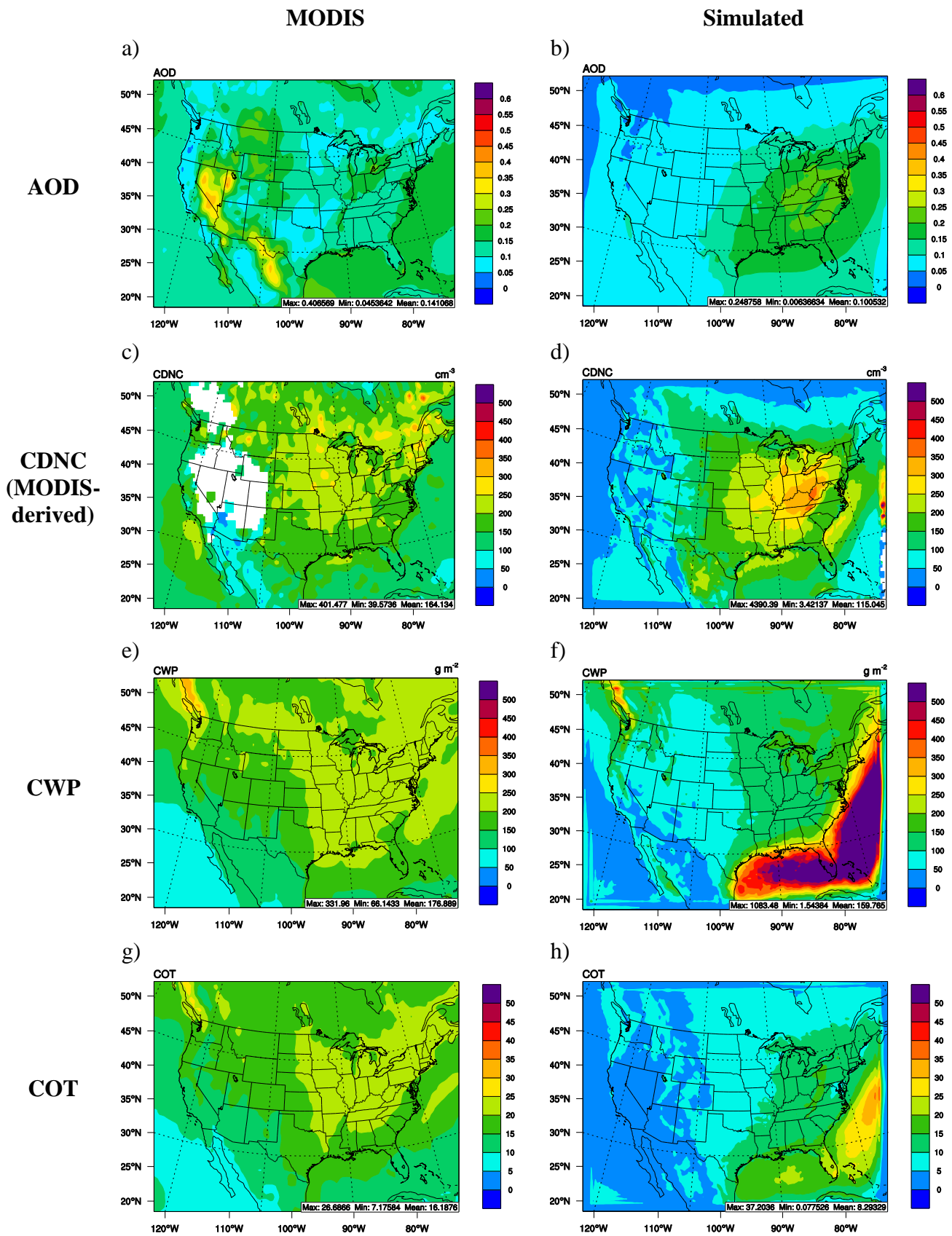


Figure 9. 10-year averaged MODIS (left) vs. simulated (right) AOD (a and b), CDNC (c and d), CWP (e and f), and COT (f and g).

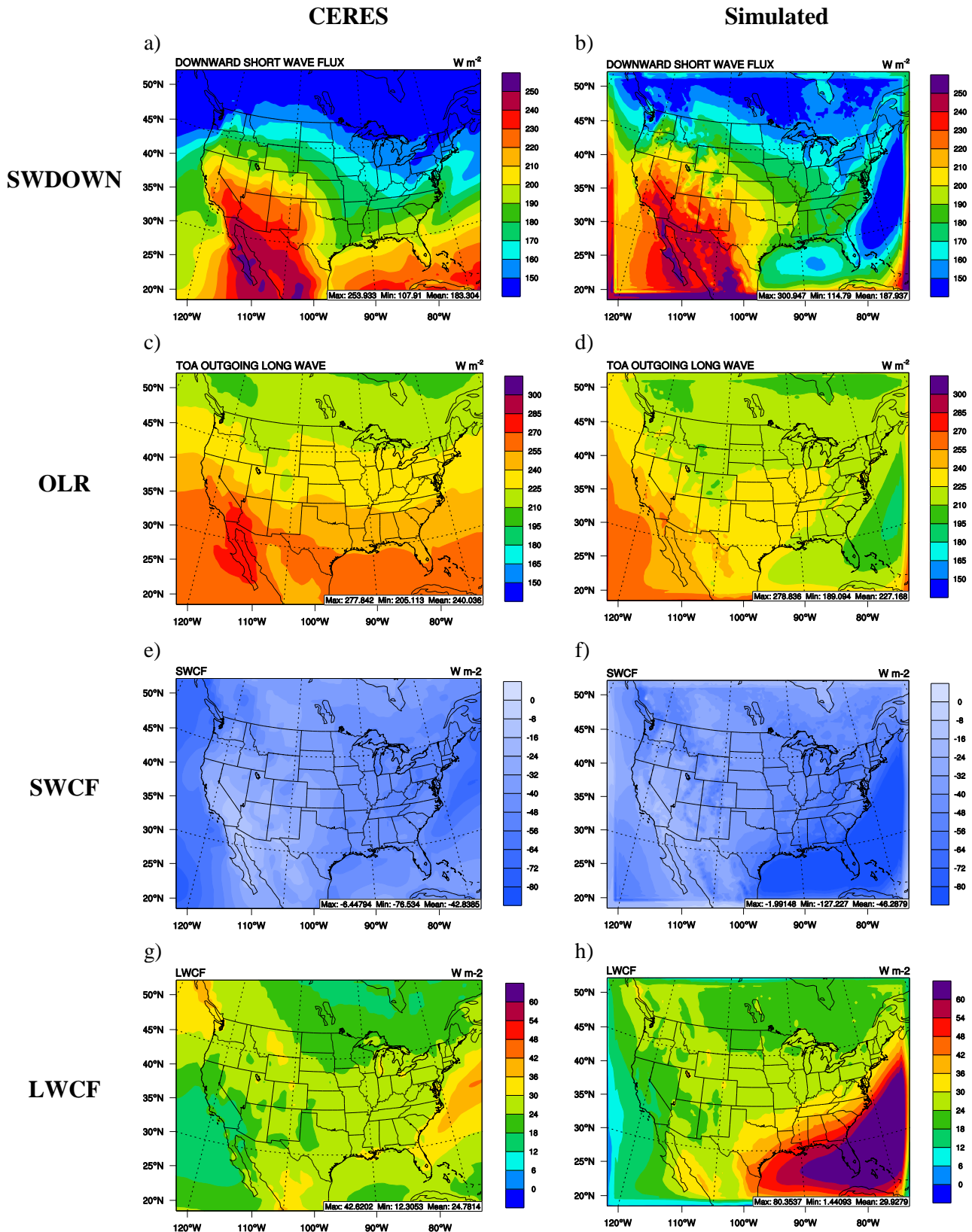


Figure 10. 10-year averaged CERES (left) vs. simulated (right) SWDOWN (a and b), OLR (c and d), SWCF (e and f), and LWCF (f and g).